

# The Importance of Priors on LIGO-Virgo Parameter Estimation: the Case of Primordial Black Holes

S. Bhagwat,<sup>a</sup> V. De Luca,<sup>b</sup> G. Franciolini,<sup>b</sup> P. Pani,<sup>a,c</sup> A. Riotto<sup>b,c</sup>

<sup>a</sup>Dipartimento di Fisica, “Sapienza” Università di Roma, Piazzale Aldo Moro 5, 00185, Roma, Italy

<sup>b</sup>Department of Theoretical Physics and Center for Astroparticle Physics (CAP)  
24 quai E. Ansermet, CH-1211 Geneva 4, Switzerland

<sup>c</sup>INFN, Sezione di Roma, Piazzale Aldo Moro 2, 00185, Roma, Italy

E-mail: [swetha.bhagwat@roma1.infn.it](mailto:swetha.bhagwat@roma1.infn.it), [valerio.deluca@unige.ch](mailto:valerio.deluca@unige.ch),  
[gabriele.franciolini@unige.ch](mailto:gabriele.franciolini@unige.ch), [paolo.pani@uniroma1.it](mailto:paolo.pani@uniroma1.it), [antonio.riotto@unige.ch](mailto:antonio.riotto@unige.ch)

**Abstract.** The black holes detected by current and future interferometers can have diverse origins. Their expected mass and spin distributions depend on the specifics of the formation mechanisms. When a physically motivated prior distribution is used in a Bayesian inference, the parameters estimated from the gravitational-wave data can change significantly, potentially affecting the physical interpretation of certain gravitational-wave events and their implications on theoretical models. As a case study we analyze primordial black holes, which might be formed in the early universe and could comprise at least a fraction of the dark matter. If accretion is not efficient during their cosmic history, primordial black holes are expected to be almost non-spinning. If accretion is efficient, massive binaries tend to be symmetrical and highly spinning. We show that incorporating these priors can significantly change the inferred mass ratio and effective spin of some binary black hole events, especially those identified as high-mass, asymmetrical, or spinning by a standard analysis using agnostic priors. The Bayes factors are only mildly affected by the new priors, implying that it is hard to distinguish whether merger events detected so far are of primordial or astrophysical origin. In particular, if binaries identified by LIGO/Virgo as asymmetrical (including GW190412) are of primordial origin, their mass ratio inferred from the data can be compatible with unity.

---

## Contents

<b>1</b>	<b>Introduction</b>	<b>1</b>
<b>2</b>	<b>PBH mass and spin distributions</b>	<b>3</b>
2.1	Without accretion	3
2.2	With accretion	3
2.3	Physically-motivated distributions of the PBH binary parameters	5
<b>3</b>	<b>Parameter estimation for coalescing BH binaries</b>	<b>8</b>
3.1	Details of the parameter estimation setup	10
3.2	Parameter estimation with PBH-motivated priors: non-accreting case	10
3.3	Parameter estimation with PBH-motivated priors: accreting case	11
<b>4</b>	<b>Results</b>	<b>12</b>
4.1	Without accretion	13
4.2	With accretion	18
<b>5</b>	<b>Conclusions</b>	<b>21</b>
<b>A</b>	<b>Parameter estimation for GW190412 in the accreting PBH scenario with <math>z_{\text{cut-off}} = 7</math></b>	<b>23</b>

---

## 1 Introduction

Following the historical breakthrough by the LIGO/Virgo Collaboration (LVC), gravitational-wave (GW) astronomy is now in full blossom. The LIGO-Virgo interferometers have so far provided us with at least 13 GW observations of candidate black-hole (BH) binaries [1, 2]. Further events from the third observational run (O3) will be released shortly and many more are expected in the future. Given the current and upcoming wealth of data, it becomes of utmost importance to confront specifics of formation models with observations and to infer the (astro)physical implications. As the number of detections increases, we will soon be in a position to address important questions like whether the observed binary BH population has the same origin or multiple formation channels.

One intriguing hypothesis is that (at least a fraction of) the merging BHs are of primordial origin, i.e., they formed early in the evolution of the universe (see Refs. [3, 4] for recent reviews). This possibility is also interesting as primordial BHs (PBHs) may comprise the totality or a fraction of the Dark Matter (DM) in the universe [5–7].

Exploring the primordial origin of GW events has motivated several works on the PBH formation mechanisms [8–11], merger rates [5, 6, 12–19], confrontation with other astrophysical constraints [20–33], and with current GW data [13, 19, 34–39]. Nonetheless, all previous studies have adopted the measurements (in particular of the masses and spins of the binary

BH components and source redshift) obtained by the Bayesian inference that uses conventional agnostic prior distributions for the binary parameters (see Sec. 3 below for details). It is well-known that a drastically different choice of priors can impact the inferred value of the parameters (i.e., their posterior distributions). In some cases, different prior assumptions might significantly change the physical interpretation of GW events [40–42]. Thus, when the parameters of the observed BHs are used to constrain, calibrate, and test physical models, the effects of priors on the inference of the parameters need to be quantified.

In this paper, we investigate the impact of the priors under the hypothesis that (at least some of) the GW events detected so far are of primordial origin. We argue that the first crucial ingredient to explore any consequence of current and future GW events for the PBH scenario is to make sure that the values of the parameters inferred from GW data (in particular BH masses and spins) are not affected by a PBH-motivated (as opposed to an agnostic) prior. As we shall show, this is indeed the case for several GW events, but not for all. We find that a PBH-motivated prior on the masses and spins can significantly affect the parameter estimation, especially the measurement of the binary mass ratio and effective spin, for those BH binaries identified as being either high-mass, or asymmetrical, or spinning using the agnostic priors. The underlying reason for this is twofold: i) the initial mass distribution of PBHs is not uniform across the mass range but depends on the physical formation mechanism that occurs in the early universe; ii) more importantly, the natal spin of PBHs is negligible, essentially restricting some of the parameters (most notably the effective spin  $\chi_{\text{eff}}$ ) in the waveform model. Unless the accretion is efficient in spinning up the PBHs during their history (see Sec. 2), a negligible-spin prior strongly affects the recovered parameters for those binaries identified as spinning by the standard LVC analysis. In particular, the inference on the mass ratio of the binary BHs are significantly modified to compensate for the absence of  $\chi_{\text{eff}}$  in the waveform and due to the different prior distribution of the masses. Furthermore, if the PBH accretion is efficient, the binaries made of heavy PBHs tend to be symmetrical and highly-spinning. This affects the posterior distributions for those binary BH events which are identified as asymmetrical or non-spinning with agnostic priors. Overall these effects can have deep consequences for the physical interpretation of some events, especially for systems like GW190412, which is identified as an asymmetrical, spinning binary using standard priors [2].

We note that while we focus on the PBH hypothesis as a case study, our results for the non-accreting case are more general and indeed apply to other scenarios (possibly of astrophysical or quantum [43] origin) in which the spin of the binary components is expected to be small.

The rest of this paper is organized as follows. In Sec. 2 we review the PBH mass and spin distributions that should be consistently adopted if one wishes to investigate the PBH scenario. Section 3 reviews aspects of the Bayesian parameter estimation and explains our method. Our results are presented and discussed in Sec. 4, whereas Sec. 5 is devoted to our conclusions. Appendix A contains some additional results for GW190412, which were omitted in the main text.

## 2 PBH mass and spin distributions

In this section we present a short summary of the main theoretical predictions for the mass and the spin distributions of PBHs. We will first focus on the scenario where no accretion is taking place, and then we analyse the consequences of a phase of accretion in the PBH cosmological evolution. The reader can find additional details in Refs. [37, 39].

### 2.1 Without accretion

The formation of a significant population of PBHs in the universe has been addressed by several models in the literature [3]. One of the most promising possibility arises in scenarios where PBHs are formed from the collapse of sizeable overdensities in the radiation dominated era [8–11]. The PBH mass distribution at the formation epoch  $z_i$  is determined by the intrinsic properties of the collapsing density perturbations, dictated by the inflationary curvature perturbations, and is usually parametrized by a lognormal distribution,

$$\psi(M, z_i) = \frac{1}{\sqrt{2\pi}\sigma M} \exp\left(-\frac{\log^2(M/M_c)}{2\sigma^2}\right), \quad (2.1)$$

in terms of its width  $\sigma$  and central mass scale  $M_c$ . This shape is often introduced to describe several models and originates when the power spectrum of the curvature perturbations generated during inflation has a symmetric peak at the small scales giving rise to the large overdensities needed to generate the PBHs upon horizon re-entry [24, 44]. We use the label "i" to indicate quantities at formation epoch.

In this common formation scenario, the nearly-spherical shape [45] of the collapsing perturbations and the small collapsing time in the radiation dominated era implies that the PBH initial spin  $\chi_i \equiv |J_i|/M_i^2$  should be below the percent level [46, 47]

$$\chi_i \sim 10^{-2} \sqrt{1 - \gamma^2}, \quad (2.2)$$

expressed as a function of the effective width of the power spectrum  $\gamma$  [46]. For example, a very peaked curvature perturbation power spectrum leads to a very narrow PBH mass function and to  $\gamma \simeq 1$ , thus further suppressing the initial PBH spin.

In the scenario in which PBHs do not undergo a phase of accretion in their cosmological evolution, their initial mass and spin distributions will be preserved up to the present epoch, as given by Eqs. (2.1) and (2.2), respectively. They therefore determine the properties of the population at the time of merger.

### 2.2 With accretion

Throughout the cosmological history, there may be periods in which baryonic mass accretion affects PBHs in binary systems, impacting their mass function [48–50] and spins [37, 39, 51]. This happens for binaries with mass  $M_{\text{tot}} \gtrsim \mathcal{O}(10)M_\odot$ , for which the binary as a whole attracts the surrounding gas as long as its typical size is smaller than its corresponding Bondi radius [37, 39]. In this situation, both the PBHs accrete baryonic particles, with individual

rates determined by their orbital velocities and their masses. The individual accretion rates are given in terms of the binary mass ratio  $q \equiv M_2/M_1 \leq 1$  as

$$\dot{M}_1 = \dot{M}_{\text{bin}} \frac{1}{\sqrt{2(1+q)}}, \quad \dot{M}_2 = \dot{M}_{\text{bin}} \frac{\sqrt{q}}{\sqrt{2(1+q)}}, \quad (2.3)$$

as a function of the Bondi-Hoyle mass accretion rate for the binary system

$$\dot{M}_{\text{bin}} = 4\pi\lambda m_H n_{\text{gas}} v_{\text{eff}}^{-3} M_{\text{tot}}^2. \quad (2.4)$$

The latter is driven by the total mass  $M_{\text{tot}} = M_1 + M_2$  and depends on the binary effective velocity  $v_{\text{eff}}$  relative to the baryons with cosmic mean density  $n_{\text{gas}}$  and the hydrogen mass  $m_H$ . The effects of the Hubble expansion, the gas viscosity, and the coupling of the CMB radiation to the gas through Compton scattering are tracked by the accretion parameter  $\lambda$ , whose explicit expression can be found in Ref. [48]. The observational constraints on the fraction of PBHs as DM, for masses larger than  $\mathcal{O}(M_\odot)$ , imply that a secondary DM-component halo should form around the isolated or binary PBHs [49, 52, 53]. Its main effect is to catalyze the gas accretion rate and is usually tracked into the accretion parameter  $\lambda$  (details are provided in App. B of Ref. [37] and references therein).

We draw the reader's attention to the fact that the accretion phase depends on the complex phenomena related to the local, global [22, 49] and mechanical [54] feedbacks, X-ray pre-heating [55] and the formation of structures [12, 56, 57]. Overall, these effects can make the accretion much less efficient at a relatively small redshift. We have decided to parametrize these uncertainties into a cut-off redshift  $z_{\text{cut-off}}$  below which accretion is negligible [37, 39], with representative values  $z_{\text{cut-off}} = \{15, 10, 7\}$ . A smaller cut-off redshift is associated to a prolonged accretion phase.

The PBH evolution is strongly affected by accretion in several aspects:

1. it induces a change of the PBH mass function according to the equation

$$\psi(M(M_i, z), z) dM = \psi(M_i, z_i) dM_i, \quad (2.5)$$

where  $M(M_i, z)$  is the final mass at redshift  $z$  for a PBH with mass  $M_i$  at redshift  $z_i$ . The evolved mass distribution is broader at higher masses and has a high-mass tail that is orders of magnitude larger than its corresponding value at formation [37];

2. it modifies the fraction of PBHs in the DM depending on the redshift with important consequences when confronting the existing constraints with the physical parameters, see Ref. [32] for details;
3. it pushes the mass ratio towards unity as  $\dot{q}/q = (\dot{M}_2/M_2 - \dot{M}_1/M_1) > 0$ , since the secondary binary component always inherits a larger accretion;
4. it influences the PBH spin evolution. Indeed, the geometry of the accretion process and the PBH spins may be crucially impacted by the angular momentum that the infalling gas particles carry [51]. In particular, the formation of a thin accretion disk [49, 58, 59]

leads to an efficient angular momentum transfer, with the consequent growth of the PBH spins with mass accretion as

$$\dot{\chi} = g(\chi) \frac{\dot{M}}{M}, \quad (2.6)$$

in terms of a function  $g(\chi)$  of the dimensionless Kerr parameter (see Refs. [39, 60–62]), until it reaches the limit  $\chi_{\max} = 0.998$  dictated by radiation effects [63, 64]. The larger accretion rates inherited by the secondary component of the binary results into a larger growth of its spin with respect to the one of the primary component.

### 2.3 Physically-motivated distributions of the PBH binary parameters

The conventional way of inferring the physical parameters of a GW model and their uncertainties is using a Bayesian inference setup, which relies on combining prior expectations of the parameter values with the likelihood from the observation to obtain a posterior distribution for the parameters (see Sec. 3 for details). In this section, we discuss the prior distributions on the relevant binary BH parameters under the hypothesis that GW events are of primordial origin.

Due to the lack of a preferred specific set of parameters for the PBH mass function, we make the assumption that all the BH coalescences detected so far are of primordial origin and determine the phenomenological values of  $M_c$  and  $\sigma$  in Eq. (2.1) which best-fit the data by performing a  $\chi^2$ -analysis [39]. Such values can be taken as the starting point of our study. When performing the analysis to find the best model for the distribution of PBH mass and spin, we used the LVC data, which adopted non-informative priors (see Sec. 3 for details). Anticipating some results discussed later on, we find that some of the posterior distributions are affected by the choice of PBH-motivated priors, which in turn can potentially modify the best-fit mass function. However, as shown in Fig. 1, we have checked that the best-fit values are stable with respect to the changes induced by re-analyzing each individual events with the PBH-motivated priors discussed in the rest of this work. This shows that our procedure is consistent. The resulting observable distributions described in Ref. [39] are not affected by the PBH-motivated choice of priors. Notice also that, since the selected values of  $f_{\text{PBH}}$  are below  $10^{-2}$ , the role of PBH clustering can be neglected [65].

After fixing the PBH model parameters with the values calibrated using the data, we now discuss the expected distributions of the physical GW observables. The easiest parameter that can be extracted from a binary BH coalescence waveform is its chirp mass,

$$M_{\text{chirp}} = \frac{(M_1 M_2)^{3/5}}{(M_1 + M_2)^{1/5}}, \quad (2.7)$$

which affects the leading-order Newtonian GW phase [66]. The first post-Newtonian correction includes the mass ratio  $q$ , whereas spin-angular momentum couplings enter to next-to-the-leading order, mainly through the binary’s effective spin parameter,

$$\chi_{\text{eff}} \equiv \frac{\chi_1 \cos \theta_1 + q \chi_2 \cos \theta_2}{1 + q}, \quad (2.8)$$

O1+O2+GW190412 - No Accretion

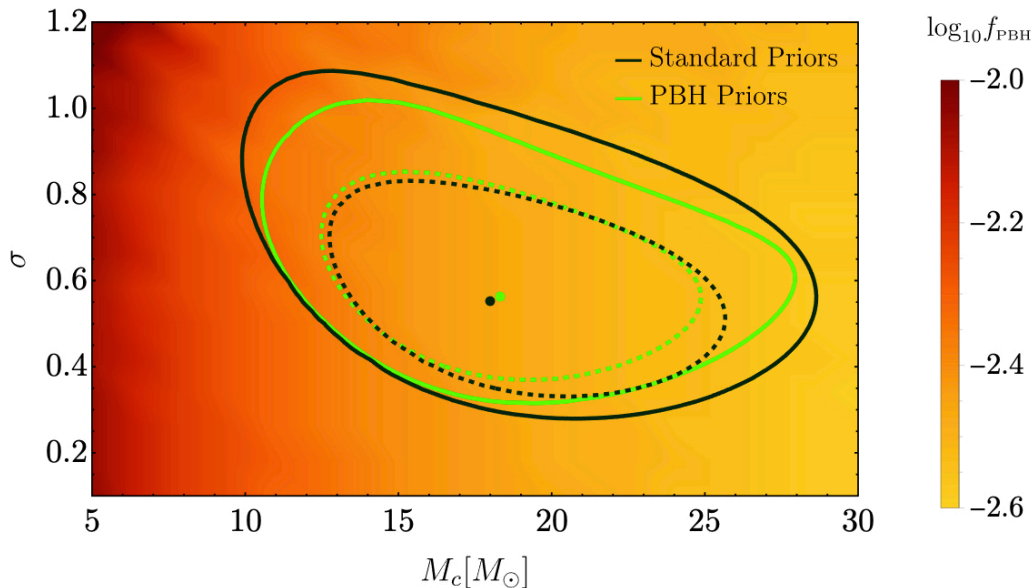


**Figure 1.**  $\chi^2$ -analysis using binary parameters (masses and source redshift) obtained with both the standard (flat) priors used by the LVC analysis and the PBH-motivated priors discussed in the following (for the case of no accretion, see Table 4). The estimation of  $M_c$  and  $\sigma$  is only mildly affected by the different choices of the priors. Here  $f_{\text{PBH}}$  is the fraction of PBHs in DM, see Ref. [39] for details.

in terms of the individual BH spins  $\chi_j$  ( $j = 1, 2$ ), and the angles  $\theta_1$  and  $\theta_2$  between the orbital angular momentum and the individual spin vectors. In the PBH scenario, we expect the spin vectors to be uniformly distributed on the two-sphere.

In Fig. 2, we show the distributions for the binary BH parameters at the formation, which coincide with the priors relevant for the parameter estimation in the case without accretion (or when accretion is inefficient). With the procedure previously outlined, the  $\chi^2$ -analysis using data from the O1-O2 runs as well as GW190412 selects the values  $M_c = 18M_\odot$  and  $\sigma = 0.55$  for the initial mass function parameters [39]. The chirp mass distribution is peaked around the central scale of the PBH mass function, with a rapid fall-off at higher masses, while the distribution of the mass ratio is quite broad. Moreover, due to the fact that the PBH spins are negligible at formation, the distribution of the effective spin parameter is very narrow around its central value  $\chi_{\text{eff}} \sim 0$ . For a reference, in this and following plots we have superimposed the corresponding values for the GW events analyzed in this paper, see Table 4 for details.

In Fig. 3 we show the priors distributions for the binary BH parameters for the case with accretion, assuming cut-off redshifts  $z_{\text{cut-off}} = \{15, 10, 7\}$ . One can see that the chirp mass distribution gets narrower with respect to the case without accretion. The mass scale at which the distribution peaks is determined by two competitive effects: i) the selection of the best-fit  $M_c$  for the initial PBH mass function which, as accretion lasts longer, peaks at

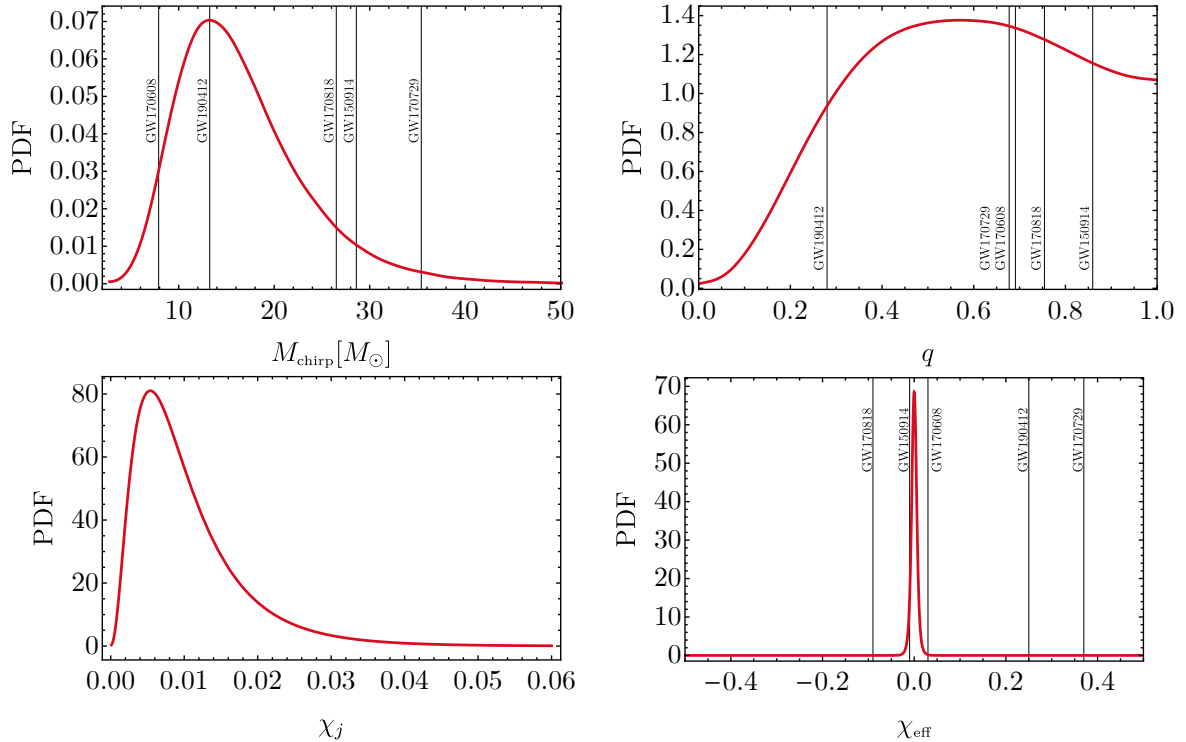


**Figure 2.** Prior distributions for the quantities  $M_{\text{chirp}}$ ,  $q$ ,  $\chi_j$  ( $j = 1, 2$ ) and  $\chi_{\text{eff}}$ , respectively, for the case of PBH binaries with no accretion. The best-fit values for the PBH mass function (Eq. (2.1)) are  $M_c = 18M_\odot$  and  $\sigma = 0.55$  [39]. For illustrative purposes, we show also the central values for the events analysed in the following (but obtained with the standard agnostic priors). Here we are showing the chirp mass values and distribution in the source-frame.

smaller values; ii) the effect of the mass evolution which pushes the distribution to higher masses. Furthermore, as discussed above, the mass ratio distribution is skewed towards the fixed point  $q = 1$  due to the accretion effects onto the binary BHs. Looking at the individual spin distributions one can appreciate that, as accretion takes place, they are also pushed towards unity, with the lighter binary component always spinning faster than the heavier one due to the characteristic behaviour of the individual mass accretion rates [39]. Furthermore, since accretion is inefficient for small masses and very efficient above a certain mass threshold, the marginalized spin distribution is bimodal with a peak at  $\chi_{1,2} \approx 0$  and another (smaller) peak towards extremality, which is anyway less relevant unless accretion is very strong. Finally, the spread of the marginalized distribution of  $\chi_{\text{eff}}$  around its central (zero) value does not change monotonically as a function of the accretion. Generically, for very strong accretion ( $z_{\text{cut-off}} \lesssim 7$ ) the distribution tends to become broader. However, intermediate cases ( $z_{\text{cut-off}} \approx 10$ ) are more involved, for example the marginalized distribution of  $\chi_{\text{eff}}$  for  $z_{\text{cut-off}} = 10$  is narrower than that for  $z_{\text{cut-off}} = 15$  for which accretion is less relevant. The reason can be understood by looking at the individual spin distributions. Due to the aforementioned bimodal shape, it is more likely to obtain intermediate values of  $\chi_{1,2}$  (and hence a broader distribution of  $\chi_{\text{eff}}$ ) for  $z_{\text{cut-off}} = 15$  than for  $z_{\text{cut-off}} = 10$ .

We stress that the spin distributions shown in Fig. 3 are marginalized over the masses.

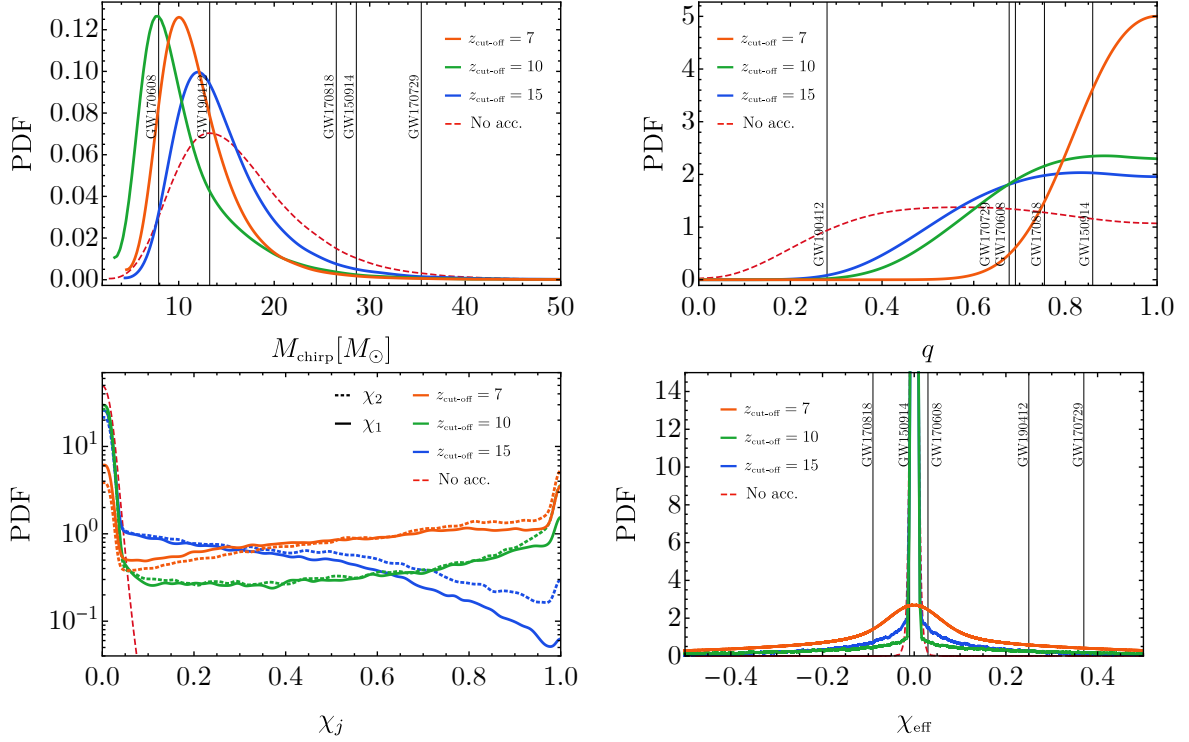


**Figure 3.** Same as Fig. 2 for the case with accretion and  $z_{\text{cut-off}} = \{15, 10, 7\}$ , where the PBH mass function is characterised by the set of parameters  $M_c = 14.1M_\odot$  and  $\sigma = 0.32$ ,  $M_c = 8.7M_\odot$  and  $\sigma = 0.29$ ,  $M_c = 7.3M_\odot$  and  $\sigma = 0.15$ , respectively [39]. As the priors have correlations between variables, the distribution shown for each individual observable is built by marginalising over all the remaining quantities.

Indeed, an additional crucial difference between the priors without and with accretion lies in the correlation between different parameters. In an accreting system, the masses and the spins of the components are intertwined, leading to a strong correlation between large chirp masses and high values of the spins. A similar, less pronounced, correlation is present between large spins (and hence a wide spread of the  $\chi_{\text{eff}}$ ) and  $q \sim 1$ . In brief, in the accreting PBH scenario high-mass binaries tend to be symmetrical and to have large spins (and hence a broad distribution of  $\chi_{\text{eff}}$  [32, 39]). This is shown in Fig. 4, a comprehensive plot to which we shall often refer to when interpreting the results of the parameter estimation in Sec. 4.

### 3 Parameter estimation for coalescing BH binaries

Bayesian parameter estimation is the conventional technique used to determine the posterior distributions  $p(\boldsymbol{\vartheta}|\mathcal{D}, \mathcal{M})$  of parameters  $\boldsymbol{\vartheta}$  in a model  $\mathcal{M}$  from the observed data  $\mathcal{D}$ . A key feature of this framework is that it folds in the expectations of distribution of the parameter values via a probability density function called the *prior*,  $\Pi = \mathcal{P}(\boldsymbol{\vartheta}|\mathcal{M})$ . The observation itself contributes to the inferred posterior distribution via a *likelihood function*  $\mathcal{P}(\mathcal{D}|\boldsymbol{\vartheta}, \mathcal{M})$ . The Bayes theorem states that the posterior probability density function  $\mathcal{P}(\boldsymbol{\vartheta}|\mathcal{D}, \mathcal{M})$  for the

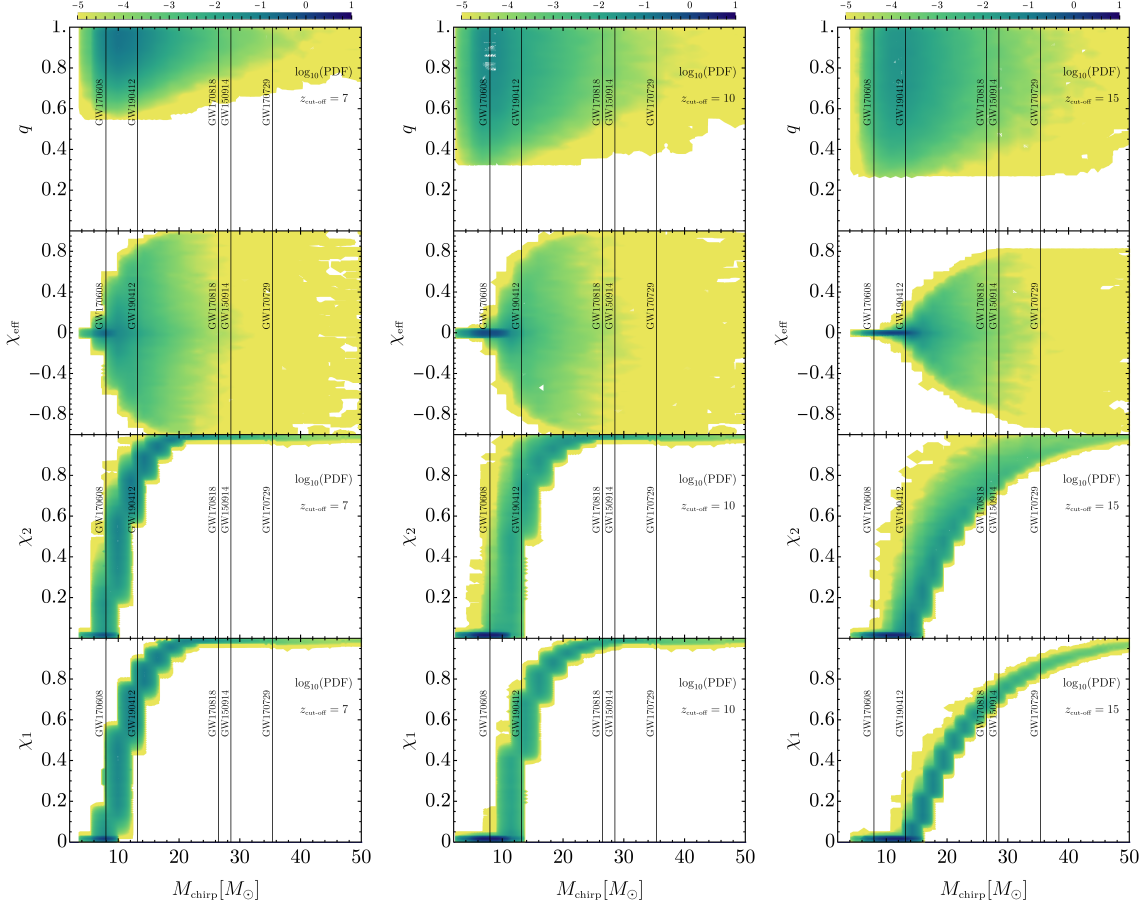


**Figure 4.** Prior distributions as in Fig. 3 in the plane  $(M_{\text{chirp}}, q)$ ,  $(M_{\text{chirp}}, \chi_{\text{eff}})$ ,  $(M_{\text{chirp}}, \chi_j)$  respectively, to show the correlation between quantities. In particular, a strong positive correlation between chirp mass and individual spins is observed, which is also inherited by  $\chi_{\text{eff}}$ . White color identifies regions with negligible values of the PDF.

parameters  $\boldsymbol{\vartheta}$  is given by [67]

$$\mathcal{P}(\boldsymbol{\vartheta}|\mathcal{D}, \mathcal{M}) = \frac{\mathcal{P}(\boldsymbol{\vartheta}|\mathcal{M})\mathcal{P}(\mathcal{D}|\boldsymbol{\vartheta}, \mathcal{M})}{Z}, \quad (3.1)$$

where  $\mathcal{D} = \mathcal{M} + \mathcal{N}$ ,  $\mathcal{N}$  is the noise, and the normalizing factor  $Z = \mathcal{P}(\mathcal{D}|\mathcal{M})$  is called the evidence. Assuming the noise model is Gaussian and stationary, the likelihood function can be expressed as

$$L = \mathcal{P}(\mathcal{D}|\boldsymbol{\vartheta}, \mathcal{M}) \propto e^{-\frac{1}{2}\langle \mathcal{N}|\mathcal{N} \rangle} = e^{-\frac{1}{2}\langle \mathcal{D} - \mathcal{M}|\mathcal{D} - \mathcal{M} \rangle}, \quad (3.2)$$

where  $\langle \cdot | \cdot \rangle$  denotes the weighted inner product. For our case,  $\mathcal{M}$  is the frequency-domain binary BH gravitational waveform  $\widetilde{h}(f)$ ,  $\mathcal{D}$  is the output of the GW interferometers expressed in the frequency domain. Further,

$$\langle \mathcal{M}|\mathcal{D} \rangle = \int_0^\infty df \frac{\widetilde{h}(f)^* \times \widetilde{\mathcal{D}}(f)}{S_n(f)}, \quad (3.3)$$

where  $S_n(f)$  is the power spectral density (PSD) of the instrument.

While the likelihood reflects the tendency of the data, the *prior*  $\mathcal{P}(\boldsymbol{\vartheta}|\mathcal{M})$  encapsulates our expectations and is a choice that is made in the inference. Furthermore, the evidence  $Z$  associated with the different choices of priors quantifies which of the prior choices is favoured by the observed data. The evidence is obtained by completely marginalizing the posterior and can be written as

$$Z = \mathcal{P}(\mathcal{D}|\mathcal{M}) = \int d\boldsymbol{\vartheta} L(\mathcal{D}|\boldsymbol{\vartheta}) \times \Pi(\boldsymbol{\vartheta}). \quad (3.4)$$

The evidence takes into account the goodness of fit of the data with the model of the signal through the  $L(\mathcal{D}|\boldsymbol{\vartheta})$  and the volume of the prior space  $\Pi(\boldsymbol{\vartheta})$ , thereby penalizing over-fitting. From a given data, if the inference is made using two or more models of the signal or the prior distributions, then the ratios of the evidences known as the Bayes factor is used to compare the performance of these assumptions. Note that this interpretation inherently assumes that each of the prior distribution is equally likely before conducting the experiment.

### 3.1 Details of the parameter estimation setup

We use the open science data for the binary BH coalescences as outlined in Ref. [68], using data from the two LIGO interferometers. We use the *BILBY* Bayesian inference library [68, 69] to perform full Bayesian parameter estimations and infer all the 15 parameters of the GW coalescence waveform model, namely the detector-frame masses ( $M_1, M_2$ ), the dimensionless spins magnitudes ( $\chi_1, \chi_2$ ) of the BHs, 4 angle variables ( $\theta_{1,2}, \delta\phi, \delta_{JL}$ ) that describe the BH spin directions, the inclination angle ( $\iota$ ), the polarization angle ( $\psi$ ), the phase at coalescence ( $\phi_c$ ), the time of coalescence ( $t_c$ ), the right ascension ( $\alpha$ ), the declination ( $\delta$ ) and the luminosity distance ( $d_L$ ). We use a dynamic nested sampler implementation called DYNESTY [70–72] within the BILBY package. The sampler is run with 1000 live points and 100 walks to produce the posterior distribution presented in Sec. 4.

For all the cases, including GW190412, we use only the dominant  $l = m = 2$  harmonic for the analysis. This is sufficient for our purposes as it is demonstrated in [73] that the inclusion of higher harmonics does not change the inferred parameter values for GW190412 (the most asymmetric binary BH system included in this analysis) significantly. IMRPhenomPv2 frequency domain waveform implementation from LALSuite [74] is used for the likelihood computations. The PSD of the detectors is calculated from the data using the GWpy package [75, 76]. A median value of PSD is used for the computation of the likelihood.

Parameter estimation is carried out for all the 15 binary BH parameters but we present only the relevant parameters in view of clarity. As explained in the previous section, the assumption of BHs having a primordial origin modifies the priors on the masses and spin magnitudes of the BHs. The implementation of these priors in the parameter estimation setup is described in Secs. 3.2, and 3.3. For all other parameters, we choose the standard non-informative priors as summarized in Table 1.

### 3.2 Parameter estimation with PBH-motivated priors: non-accreting case

If accretion during the cosmological evolution of PBHs is not efficient, their masses and spins are those at formation. As previously discussed, for the former we use the log-normal

Parameter	Prior
$\theta_{i,j}$	Sin prior in $[0, \pi]$
$\delta\phi$	Uniform prior in $[0, 2\pi]$
$\delta_{JL}$	Uniform prior in $[0, 2\pi]$
$t_c$	Uniform prior around the event trigger time
$\phi_c$	Uniform in $[0, 2\pi]$
$\alpha$	Uniform prior in $[0, 2\pi]$
$\delta$	Cosine prior in $[-\pi/2, \pi/2]$
$d_L$	Power law prior in $[50, 2000]$ Mpc
$\iota$	Sin prior in $[0, \pi]$
$\psi$	Uniform in $[0, 2\pi]$

**Table 1.** List of the standard, non-informative priors we use for 11 (out of 15) waveform parameters. The PBH-motivated priors on the BH masses and spins are summarized in Table 2.

	PBH-motivated priors (no accretion)	Standard (LVC) Priors
$M_1$	Lognormal with $M_c = 18M_\odot$ and $\sigma = 0.55$	Uniform, $M_1 \in [3, 30]M_\odot$
$M_2$	Lognormal with $M_c = 18M_\odot$ and $\sigma = 0.55$	Uniform, $M_2 \in [3, 30]M_\odot$
$\chi_1$	Gaussian with $\mu = 0.005$ and $\sigma = 0.002$	Uniform, $\chi_1 \in [0, 0.99]$
$\chi_2$	Gaussian with $\mu = 0.005$ and $\sigma = 0.002$	Uniform, $\chi_2 \in [0, 0.99]$

**Table 2.** Summary of the standard priors adopted by the LVC analysis and those motivated by a PBH scenario without accretion for the binary masses and spin. The lognormal distribution for the PBH masses is defined in Eq. (2.1), whereas we approximate the spin distribution by a Gaussian with central value  $\mu$  and spread  $\sigma$ .

distribution given in Eq. (2.1) with parameters  $M_c$  and  $\sigma$  obtained by a population-driven analysis as discussed in Sec. 2.3, assuming all O1+O2+GW190412 events detected so far are of primordial origin [39]. The real distribution for the spins is complicated [46] and we approximate it by a Gaussian with central value  $\mu = 0.005$  and standard deviation  $\sigma = 0.002$ . In our analysis, we have checked that the specific form of the distribution is irrelevant as long as it only has effective support for  $\chi_{1,2} \lesssim 0.01$ , as predicted by the formation scenario [46]. A comparison between the PBH-motivated priors and the agnostic ones adopted by the LVC analysis is presented in Table 2. Finally, since the spin orientations are unknown in most scenarios, in all cases we assume that the spin vectors are isotropically distributed.

### 3.3 Parameter estimation with PBH-motivated priors: accreting case

As discussed in Sec. 2.2, if accretion is relevant during the cosmological evolution of the PBHs, the masses and the spins of the BHs evolve. As a consequence, the distributions of the masses and the spins of the BHs observed by the detectors are correlated when the binary BH enters the LIGO-Virgo band.

When accretion is significant, one would ideally need to implement a *conditional* priors. In other words, unlike the cases of non-accreting PBH priors or agnostic priors, the

Parameter	$z_{\text{cut-off}} = 7$	$z_{\text{cut-off}} = 10$	$z_{\text{cut-off}} = 15$
$M_1$	$M_c = 15.78M_\odot$ $\sigma = 0.109$	$M_c = 17.03M_\odot$ $\sigma = 0.138$	$M_c = 17.56M_\odot$ $\sigma = 0.152$
$M_2$	$M_c = 14.122M_\odot$ $\sigma = 0.109$	$M_c = 13.31M_\odot$ $\sigma = 0.138$	$M_c = 13.197M_\odot$ $\sigma = 0.152$

**Table 3.** Parameters of the lognormal prior distribution for PBH masses  $M_1$  and  $M_2$  with significant accretion for the representative cases  $z_{\text{cut-off}} = 7, 10$  and  $15$ .

prior distribution  $\Psi = \Psi(M_1, M_2, \chi_1, \chi_2)$  for accreting PBHs cannot be factorized as  $\Psi = \Psi_a(M_1)\Psi_b(M_2)\Psi_c(\chi_1)\Psi_d(\chi_2)$ .

However, the practical implementation of conditional priors is challenging and involves handling multi-dimensional interpolated prior functions. Most nested samplers implementation involve taking the inverse cumulative distribution function of the prior distribution and this can be complicated for a generic parameter correlation. This is especially a problem if the multidimensional priors have sharp features, which is our case in some parts of the parameter space. Finally, the distribution  $\Psi(M_1, M_2, \chi_1, \chi_2)$  is not known in an analytical form and have to be tabulated numerically.

To overcome these difficulties, in the case of accreting PBHs we have adopted the following approximate procedure. For a given accretion cut-off  $z_{\text{cut-off}}$ , we build a Monte Carlo simulation of the PBH population, from which we measure the exact mass function in tabulated form. The latter is independent of the values of the spins and of other parameters. Then, we approximate the numerical mass function with the log-normal distribution given in Eq. (2.1), with parameters  $M_c$  and  $\sigma$  obtained by fitting (see Table 3).

To construct manageable spin priors in a factorized form, for each event, we accounted for the correlation of  $\chi_{1,2}$  with the masses by building their approximate distribution considering only the events in the simulation constrained to have  $M_{\text{chirp}}$  within the corresponding GW event chirp mass 90% C.I. (as inferred with standard priors). We expect this to be accurate since the chirp mass, when performing the parameter estimation, does not correlate strongly with other parameters and is indeed much less sensitive to the choice of different priors. Thus, our approximation should be valid as long as the value of  $M_{\text{chirp}}$  inferred by using PBH-motivated priors does not differ significantly from that inferred by using agnostic priors, as can be checked a posteriori. The spin priors obtained through this procedure are shown in Fig. 5 for the representative case of GW190412. We use these numerical tabulated priors in our analysis of the accreting PBH scenario.

## 4 Results

In this section we present the results of the parameter estimation for some representative GW events by implementing the PBH-motivated priors discussed in Sec. 2 in the BILBY infrastructure [68, 69] and performing the analyses presented in Sec. 3. We discuss the scenarios with and without accretion separately.

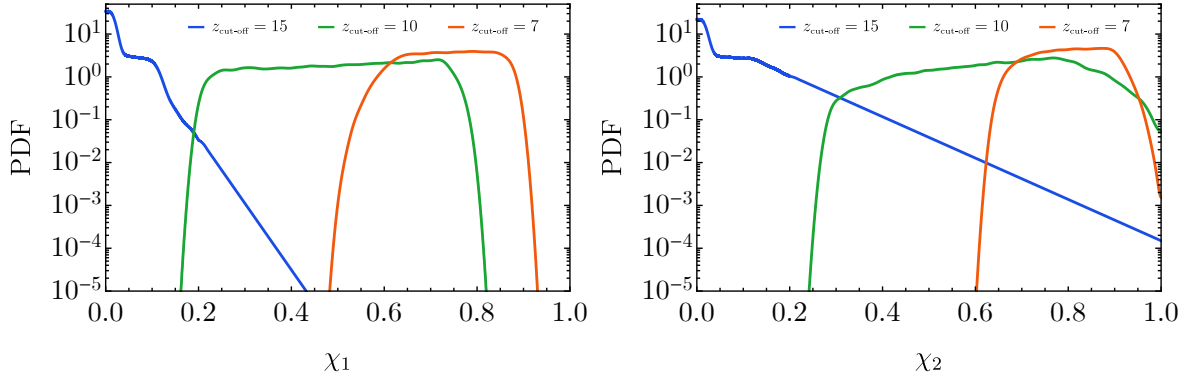


**Figure 5.** Prior distributions for PBH spins, for GW190412 parameter estimation, with significant accretion for  $z_{\text{cut-off}} = 7, 10, 15$ .

#### 4.1 Without accretion

We divide the events thus far detected by the LVC [1, 2] into 4 categories and study one event in each category for the case of priors corresponding to PBHs without accretion as well as for the standard agnostic priors. In particular, we consider (see Table 4):

1. GW150914 [77], as representative for moderate mass, symmetrical, binary BH systems;
2. GW170608 [78], as representative for low mass, symmetrical, binary BH systems;
3. GW170729 [1], as representative for moderate mass, asymmetrical, binary BH systems;
4. GW190412 [2], as representative for low mass, asymmetrical, binary BH systems.

We distinguish between low-mass and moderate-mass binaries (depending on whether  $M_{1,2} \lesssim 20M_{\odot}$ ), between symmetrical and asymmetrical systems (depending on whether  $q$  is compatible with unity, at least marginally within the errors, or not), and between non-spinning and spinning binaries (depending on whether the posterior distribution of  $\chi_{\text{eff}}$  is compatible with zero or not). We stress that these parameters refer to the original ones obtained with the standard priors on the masses and the spins adopted by the LVC (see Table 2). Further, since GW150914 was a very loud detection, we also study GW170818 to better understand the effect of the priors for a less loud event belonging to the first category.

The results of the Bayesian inference for these systems performed by implementing the priors in Table 2 within the BILBY infrastructure are presented below. Figure 6 shows a corner plot with relevant parameters for GW150914, which is the prototypical example of a moderate-mass, symmetrical binary with a high signal-to-noise ratio [77]. In the case of the standard priors, we recover the LVC results for the posterior distributions of the parameters (green curves). With the PBH-motivated priors without accretion (magenta curves), the effective spin is assumed to be essentially zero, so its posterior simply reflects the very narrow prior. In turn, this provides a slightly better measurement of the chirp mass, since the dimensionality of the waveform parameter space is effectively reduced. However, in the case of GW150914 the chirp mass is only mildly affected by the different choice of

		<b>GW150914</b>	<b>GW170818</b>	<b>GW170608</b>	<b>GW170729</b>	<b>GW190412</b>
		Moderate mass, Symmetrical, Non-spinning	Moderate mass, Symmetrical, Non-spinning	Low mass, Symmetrical, Non-spinning	Moderate mass, Asymmetrical, Spinning (?)	Low mass, Asymmetrical, Spinning
<b>Parameter</b>	<b>Prior</b>					
$M_{\text{chirp}}$	Standard PBH	$30.63^{+1.40}_{-1.48}$	$32.45^{+2.63}_{-2.64}$	$8.50^{+0.03}_{-0.03}$	$50.54^{+8.64}_{-8.96}$	$15.21^{+0.28}_{-0.27}$
		$31.15^{+0.45}_{-0.47}$	$32.78^{+0.69}_{-0.94}$	$8.47^{+0.01}_{-0.01}$	$41.47^{+3.01}_{-3.16}$	$15.12^{+0.16}_{-0.27}$
$M_1$	Standard PBH	$34.66^{+4.77}_{-2.66}$	$35.15^{+8.87}_{-5.37}$	$11.49^{+4.02}_{-2.02}$	$58.61^{+14.88}_{-11.97}$	$28.90^{+5.15}_{-5.24}$
		$35.43^{+4.12}_{-2.55}$	$34.31^{+7.75}_{-4.61}$	$9.53^{+0.80}_{-0.48}$	$56.06^{+11.15}_{-12.07}$	$18.87^{+3.26}_{-3.37}$
$M_2$	Standard PBH	$29.86^{+2.87}_{-4.19}$	$25.30^{+5.17}_{-5.99}$	$7.35^{+1.43}_{-1.71}$	$35.79^{+13.58}_{-11.97}$	$8.40^{+1.65}_{-1.04}$
		$30.40^{+2.87}_{-4.19}$	$26.18^{+4.42}_{-5.54}$	$8.65^{+0.45}_{-0.68}$	$26.5^{+8.98}_{-5.89}$	$11.98^{+2.57}_{-1.78}$
$q$	Standard PBH	$0.86^{+0.12}_{-0.20}$	$0.72^{+0.25}_{-0.27}$	$0.64^{+0.28}_{-0.28}$	$0.6^{+0.35}_{-0.24}$	$0.29^{+0.13}_{-0.07}$
		$0.86^{+0.12}_{-0.17}$	$0.77^{+0.21}_{-0.26}$	$0.91^{+0.08}_{-0.13}$	$0.47^{+0.32}_{-0.14}$	$0.63^{+0.30}_{-0.16}$
$\chi_{\text{eff}}$	Standard PBH	$-0.06^{+0.10}_{-0.13}$	$-0.05^{+0.19}_{-0.22}$	$0.06^{+0.14}_{-0.05}$	$0.29^{+0.22}_{-0.27}$	$0.22^{+0.09}_{-0.11}$
		$0.00^{+0.00}_{-0.00}$	$0.00^{+0.00}_{-0.00}$	$0.00^{+0.00}_{-0.00}$	$0.00^{+0.01}_{-0.01}$	$0.00^{+0.00}_{-0.00}$
$z$	Standard PBH	$0.10^{+0.03}_{-0.04}$	$0.26^{+0.09}_{-0.10}$	$0.07^{+0.02}_{-0.02}$	$0.29^{+0.07}_{-0.13}$	$0.17^{+0.03}_{-0.06}$
		$0.09^{+0.03}_{-0.04}$	$0.26^{+0.09}_{-0.11}$	$0.07^{+0.03}_{-0.03}$	$0.26^{+0.09}_{-0.13}$	$0.17^{+0.04}_{-0.07}$
$\log \mathcal{B}$	Standard PBH	$280.0 \pm 0.1$	$43.0 \pm 0.1$	$87.3 \pm 0.2$	$44.1 \pm 0.1$	$146.7 \pm 0.2$
		$279.0 \pm 0.2$	$42.3 \pm 0.1$	$88.7 \pm 0.2$	$40.1 \pm 0.1$	$144.8 \pm 0.2$

**Table 4.** Summary of the GW events analyzed with PBH-motivated priors ignoring accretion effects. Each event is representative of a class (low/moderate mass, (a)symmetrical, (non)spinning binaries). We show the median values of the binary parameters obtained with the standard (flat) priors on the masses and spins adopted by the LVC and with the PBH-motivated priors neglecting accretion. The last row presents the log Bayes factors obtained in the two cases for each event. Errors represent the 90% confidence intervals.

the priors (and anyway the new posterior is well within the  $1\sigma$  contour of the standard one), whereas the posterior distribution of the mass ratio is almost unaffected. This can be understood by noticing that the effective spin parameter of GW150914 as measured by the LVC is compatible with zero, so a narrow prior  $\chi_{\text{eff}} \approx 0$  is compatible with the measurement and does not affect the inference on the other parameters. Likewise, the chirp mass estimated for GW150914 is well within the best-fit lognormal distribution inferred for PBHs (see Fig. 2). Overall, for GW150914 the effect of the PBH-motivated priors without accretion is negligible. Although we do not explicitly show the inference plots for GW170818 [1], We find very similar results also for this system, which has the same qualitative features as GW150914.

The results of the analysis of GW170608 [78] are shown in Fig. 7. In this case we observe three effects: (i) the standard posterior distribution of  $\chi_{\text{eff}}$  is peaked slightly off zero, although  $\chi_{\text{eff}} \approx 0$  is still compatible with it and hence not necessarily in tension with the negligible-spin prior; (ii) besides being more narrow as in the case of GW150914, the mass distribution arising from the PBH prior is also peaked towards slightly smaller values compared to the standard prior case; (iii) the combination of these effects conspires to impact on the posterior distribution of  $q$  more significantly. In particular, the PBH priors yield a more accurate measurement which is skewed towards larger values (median  $q = 0.91^{+0.08}_{-0.13}$ ), although still compatible with the standard-prior case within the errors.

In Fig. 8 we show the results for GW170729 [1].<sup>1</sup> In this moderate-mass case the

<sup>1</sup>We note that in this case, using the standard LVC priors, we obtain posterior distributions which are

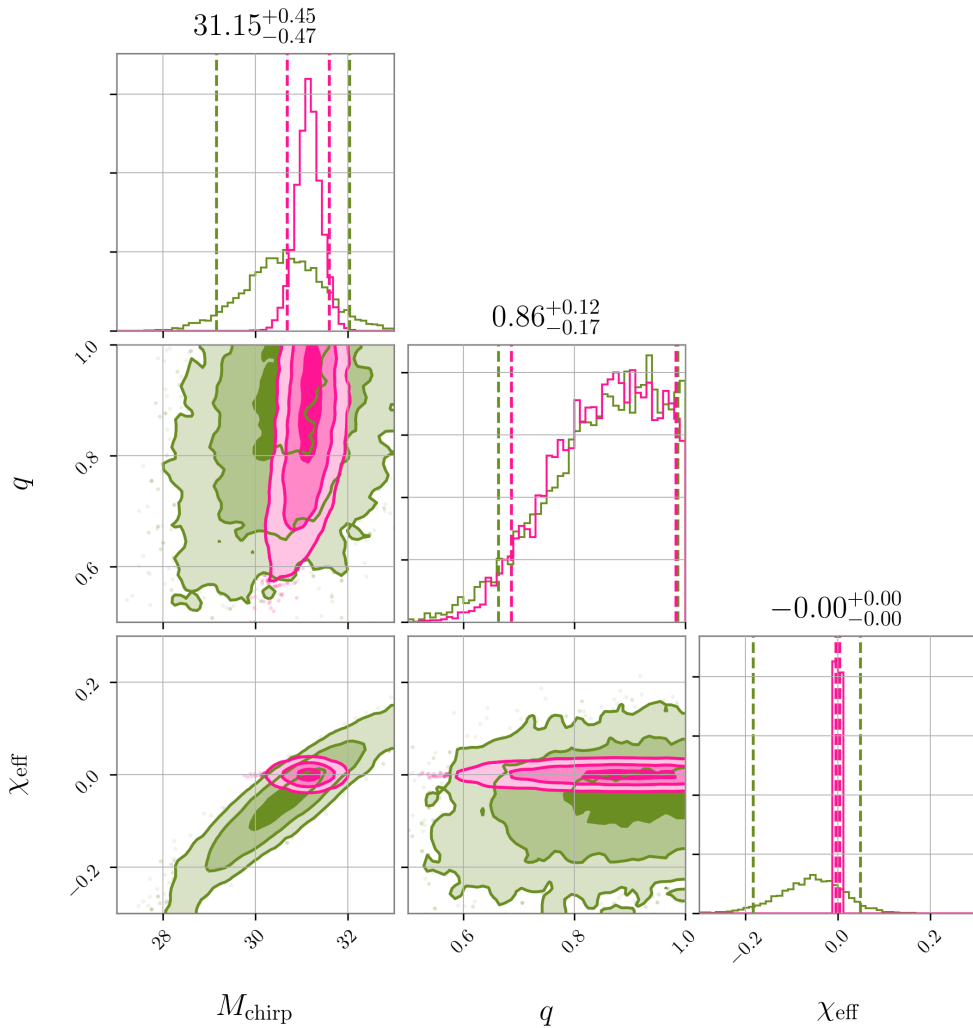


**Figure 6.** Corner plot for the relevant binary BH parameters of GW150914. The posterior distributions obtained with the PBH-motivated priors without accretion for the masses and spins correspond to the magenta contours, whereas the green curves correspond to the posterior obtained with standard priors used in the LVC analysis. The values quoted on the one-dimensional histogram correspond to the PBH-motivated priors.

standard analysis provides a moderate value for the median of  $\chi_{\text{eff}}$  (although  $\chi_{\text{eff}} = 0$  is not excluded) and a mass ratio which is significantly smaller than unity (although with large uncertainties). Here, we observe the same qualitative effects as in the previous cases: namely the PBH-motivated priors yield a slightly lower chirp mass with smaller errors, and also affect the mass ratio which is correlated to  $\chi_{\text{eff}}$ .

Finally, in Fig. 9 we present the results for GW190412, the first binary BH event published from the O3 run [2]. This event is particularly interesting for our study because it was confidently identified as a spinning ( $\chi_{\text{eff}} = 0.22^{+0.09}_{-0.11}$ ) and asymmetric ( $q = 0.29^{+0.13}_{-0.07}$ )

slightly different from those reported by the LVC. However, uncertainties for this system are large and the inferred values significantly depend on the analysis, including the waveform model [79].

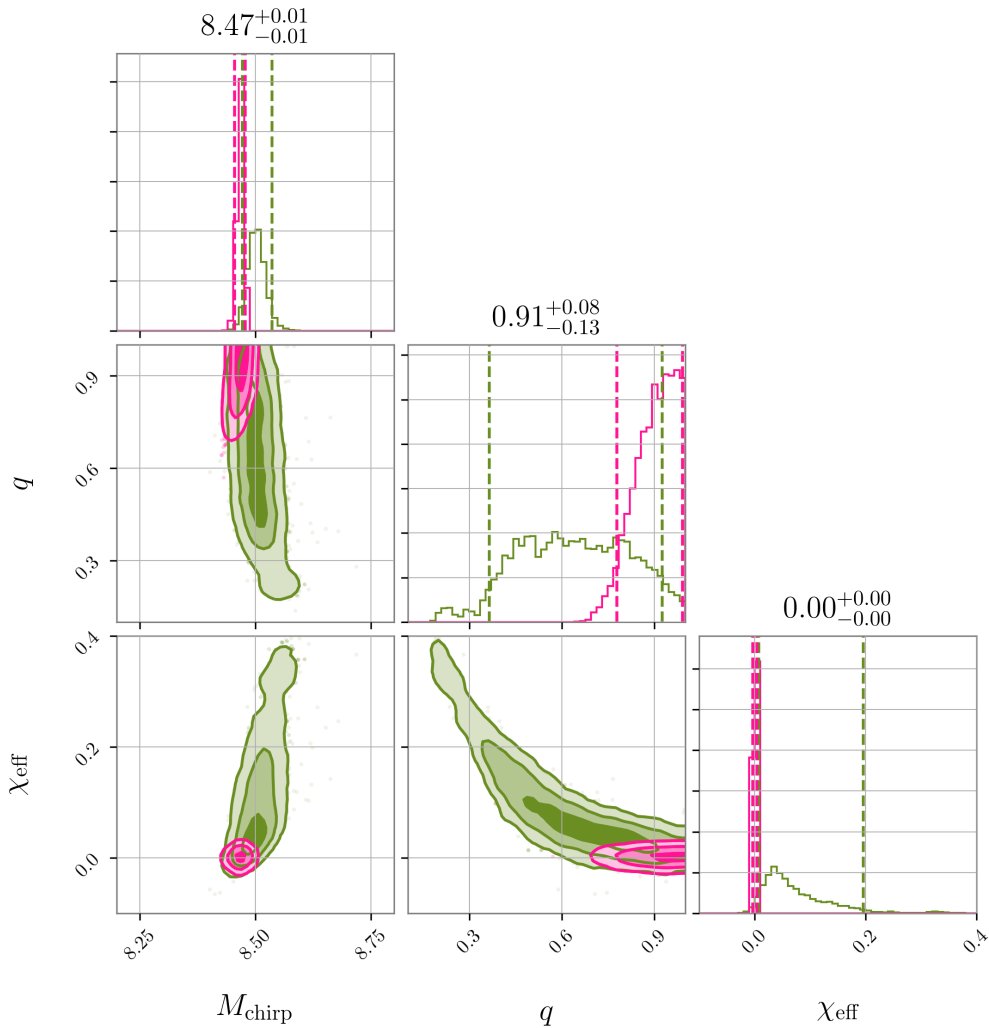


**Figure 7.** Same as in Fig. 6 but for GW170608.

binary by the LVC analysis. However, these measurements rely on the standard (agnostic) choice for the mass and the spin priors, whereas a different prior assumption might change the qualitative nature of the inferred binary BH parameters [41, 42].

As compared to the other cases, GW190412 presents some peculiarities. Being a low-mass binary system, its chirp mass inferred using the agnostic prior is also compatible with the PBH-motivated priors, so the two posteriors for  $M_{\text{chirp}}$  as shown in Fig. 9 are very similar. However, in this case  $\chi_{\text{eff}} = 0$  is excluded roughly at  $3.3\sigma$  confidence level if one adopts the standard flat priors on the spins. This is in tension with the PBH-motivated prior without accretion which imposes  $\chi_{\text{eff}} \approx 0$ . Consequently, the measurement of the mass ratio is strongly affected in order to compensate for this tension, since  $q$  and  $\chi_{\text{eff}}$  are correlated in the waveform. Specifically, the distribution of  $q$  gains support close to unity and broadens up: while with standard priors GW190412 can be confidently identified as a strongly asymmetric binary, the PBH-motivated priors give a distribution which is also compatible (within less

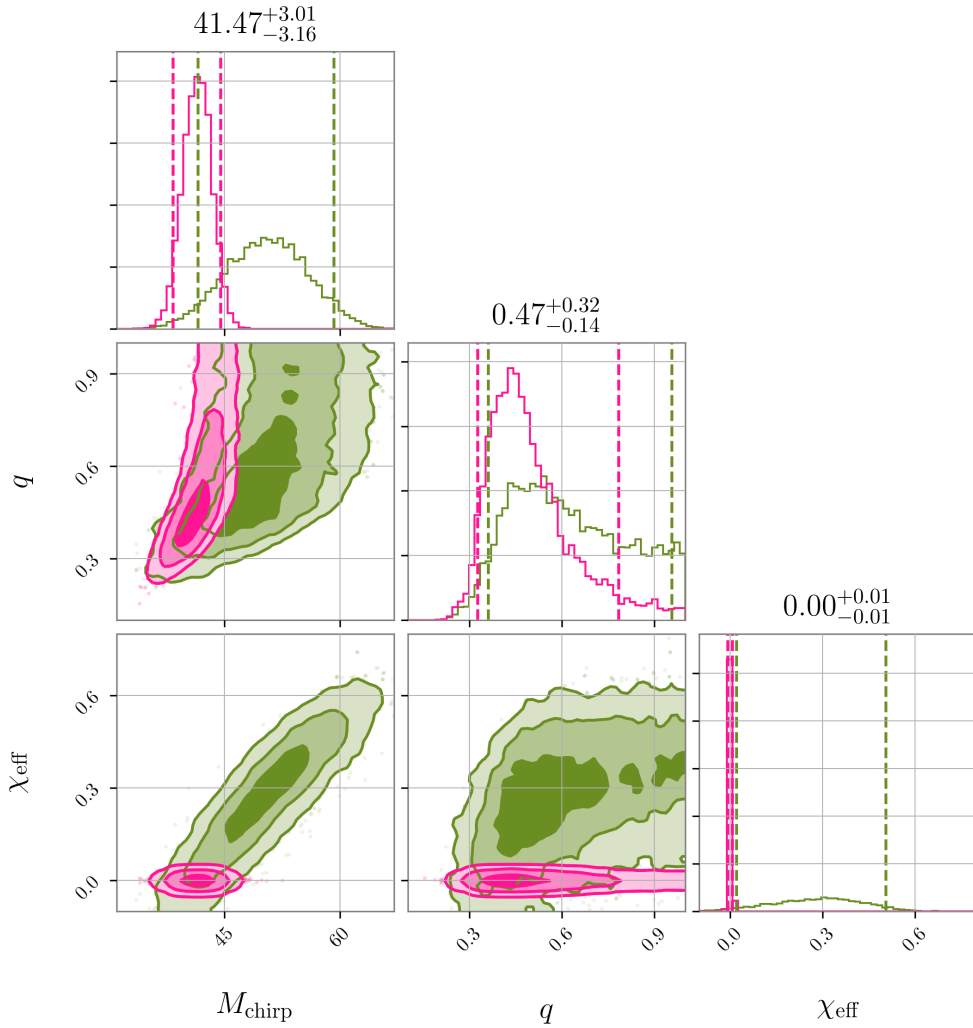


**Figure 8.** Same as in Fig. 6 but for GW170729.

than  $2\sigma$  confidence level) with a perfectly symmetric binary ( $q = 1$ ). We expect that this is a generic result that should apply to any binary for which the distribution of  $\chi_{\text{eff}}$  (as inferred using standard priors) is incompatible with zero. If in addition the mass of the binary is large, there might be other effects due to different posterior distributions of  $M_{\text{chirp}}$ , unlike in the case of GW190412.

Although not shown in the corner plot, one of the parameters of the waveform model is the luminosity distance, from which the redshift of the source can be inferred. As shown in Table 4, the redshift is almost insensitive to the different choice of the priors.

Finally, one can compute the Bayes factors for the presence of a signal against noise, as explained in Sec. 3. These are presented in the last row of Table 4 for the GW events considered above. Larger the value in this row, more is the preference of the data towards that prior model. Interestingly enough, for most of the cases the Bayes factors do not disfavor the hypothesis of the BH events being of primordial origin strongly. All events considered in

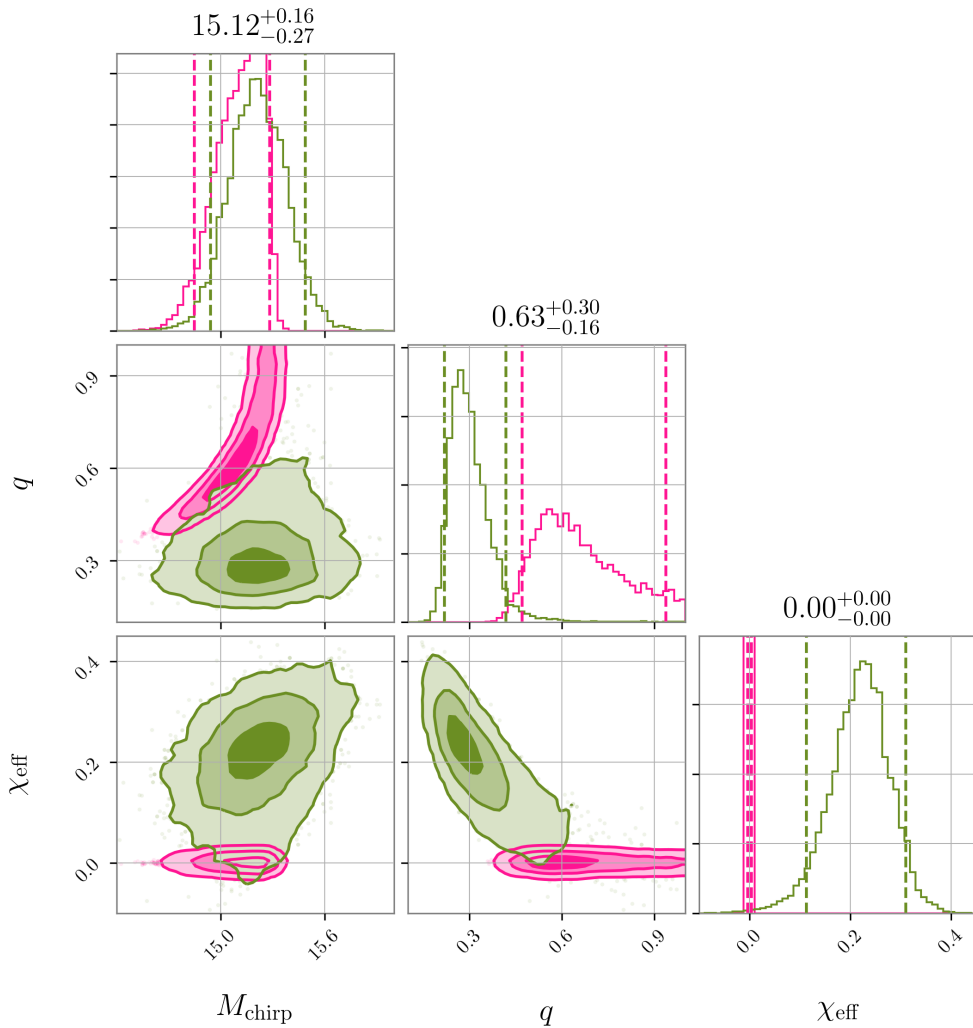


**Figure 9.** Same as in Fig. 6 but for GW190412.

our analysis – with the exception of GW170608 – show a weak statistical preference for the standard priors.

## 4.2 With accretion

As discussed in Sec. 2.2, an efficient phase of accretion during the cosmic history of PBHs affects the distribution of the individual masses and spins at detection [32, 37], and also modifies the best-fit values of a given mass function as obtained from the likelihood analysis of the observed events under the hypothesis that the latter are of primordial origin [39]. Furthermore, in the case of accretion the spin prior distributions are correlated with those of the masses. Thus, while it is straightforward to implement the exact prior distributions for the masses, those of the spins are more involved. As explained in Sec. 3.3, we adopted approximated spin distributions which account for the mass/spin correlation and are derived by fixing the chirp mass as inferred by a standard analysis. We expect this approximation to

be accurate as long as  $M_{\text{chirp}}$  does not change significantly with different prior choices, which can be checked a posteriori and is indeed our case.

The approximated spin prior distribution can be read off the panels in Fig. 4. For moderate-mass events (like GW150914, GW170818, and GW170729), the spin distribution peaks always near extremality and is very narrow (being these events above the mass-threshold for accretion), at least for small values of  $z_{\text{cut-off}}$ . In the case of moderate accretion ( $z_{\text{cut-off}} = 15$ ) the distribution of the spin is less extreme, but nonetheless centered around high values and without support at small spins. This implies that the prior distribution of  $\chi_{\text{eff}}$  is broad for these systems (since the angles are unknown, see second row in Fig. 4) and can easily accommodate any measurement. On the other hand, for light binaries (like GW170608) accretion is always inefficient and therefore, the spin distribution is similar to the non-accreting case, being sharply peaked at  $\chi_{1,2} \approx 0$ . As show in Fig. 4, the case of GW190412 is in between these two regimes: in this case we expect that the spin distribution should depend strongly on  $z_{\text{cut-off}}$ : for  $z_{\text{cut-off}} = 15$  the spins are small as in the non-accreting case, whereas for  $z_{\text{cut-off}} = 7$  the spins are moderately high with no support at  $\chi_{1,2} = 0$ , see also Fig. 5.

This preliminary analysis suggests that the effect of accretion can be understood by performing the parameter estimation for GW190412 with different values of  $z_{\text{cut-off}}$  as representative examples. This is done in Fig. 10, where we show the usual corner plot for two cases:  $z_{\text{cut-off}} = \{10, 15\}$  (see Appendix A for the case  $z_{\text{cut-off}} = 7$ ). The PBH-motivated priors including accretion correspond to the purple curves. For comparison, we also show the previous cases of standard agnostic priors (green curves) and of PBH-motivated priors without accretion (magenta curves).

For  $z_{\text{cut-off}} = 15$  (top corner plot of Fig. 10), accretion is small and the spin prior distributions are centered around zero (see right panels of Fig. 4 and Fig. 5 and notice that the scale of the density function in Fig. 4 is logarithmic). Thus, in this case we observe the same effect as in the non-accreting case. Namely, the posterior distribution of  $\chi_{\text{eff}}$  is centered around zero (although is broader than in the non-accreting case) and – as a consequence – the mass-ratio posterior moves to higher values closer to unity, with a distribution similar to the non-accreting PBH case.

On the other hand, already for  $z_{\text{cut-off}} = 10$  (bottom corner plot of Fig. 10) the effect of accretion is much stronger: in this case the individual spin distributions are typically high and yields a very broad distribution on  $\chi_{\text{eff}}$  (see second row of Fig. 4). In this case, the constraining power of  $\chi_{\text{eff}}$  is strongly reduced, since the prior can accommodate almost any value. Nonetheless, from the bottom panel of Fig. 10 we observe that the posterior distribution of the mass ratio and of the effective spin are different from those obtained with the standard agnostic priors. This is due to the peculiar prior distribution of  $q$ : strongly accreting binaries tend to be symmetrical and therefore the priors on  $q$  are skewed towards unity, being in tension with the measurement of  $q$  inferred for GW190412 with standard priors. Thus, compared to the non-accreting PBH scenario (in which the posterior on  $q$  is modified to compensate for a narrow prior on  $\chi_{\text{eff}}$  which is in tension with the data), in the strongly-accreting PBH scenario the opposite occurs: higher values of  $q$  are favored by the priors and also  $\chi_{\text{eff}}$  is

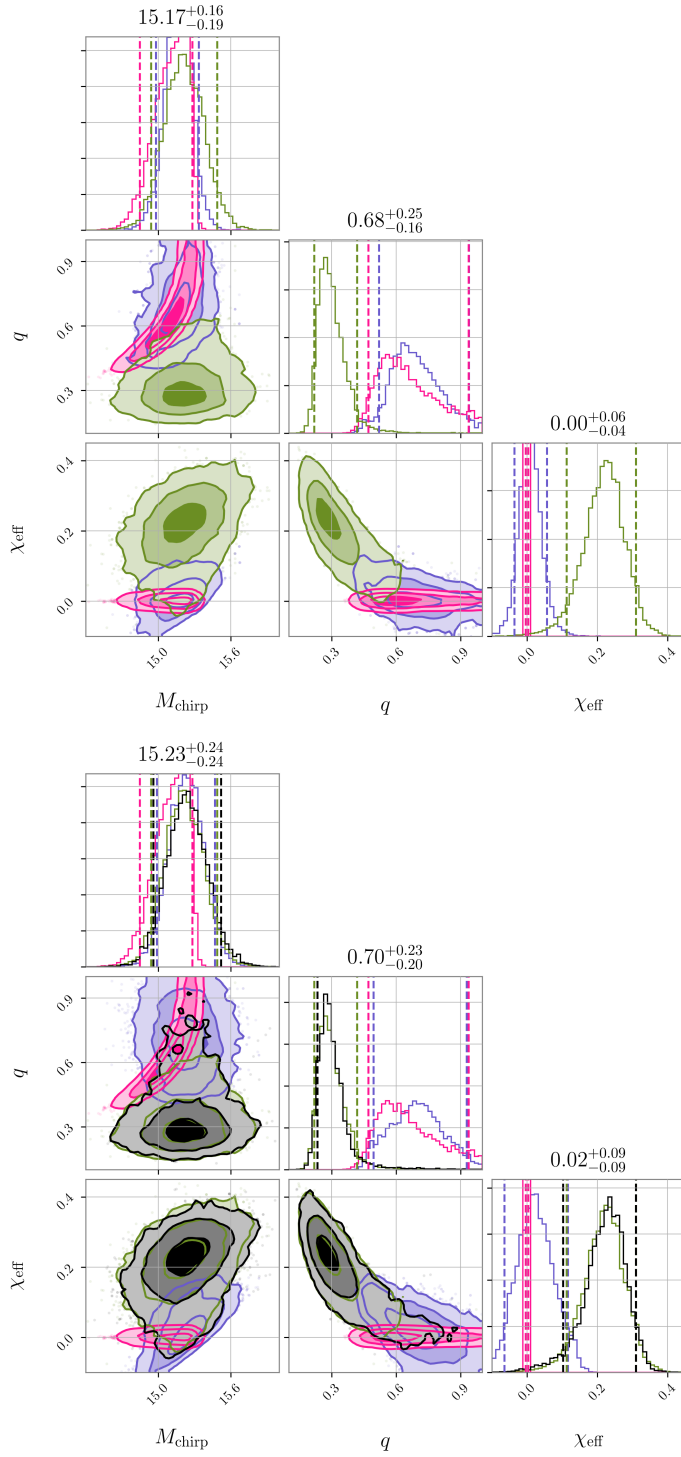


**Figure 10.** Corner plot for GW190412 including the case of PBH-motivated priors with accretion. The upper (lower) corner plot refers to  $z_{\text{cut-off}} = 15$  ( $z_{\text{cut-off}} = 10$ ), whereas the similar case of  $z_{\text{cut-off}} = 7$  is presented in Appendix A for completeness. The purple curves correspond to the accreting PBH priors on masses and spins. For reference, the green curves correspond to standard (flat) priors, whereas the magenta curves correspond to the non-accreting PBH scenario (see Fig. 9). For the  $z_{\text{cut-off}} = 10$  case we also show the mixed case (black curves) corresponding to spin priors obtained in the accreting scenario but with a flat agnostic prior on the masses, see discussion in the text. The values on the 1-d histograms correspond to the case where we use the full accretion priors (purple curves).

modified to compensate for this difference. We expect this to be a generic feature for those binaries identified as highly asymmetrical using agnostic priors.

To check this expectation, we have repeated the parameter estimation of GW190412 using a *mixed*, unphysical choice of the priors: namely, we used the accreting PBH-motivated priors for the spins but standard (flat) priors for the masses. The result is shown in the bottom corner plot of Fig. 10 by the black curves. In this case the posterior distribution is very similar to the standard one, since the prior distributions are compatible with each other.

In all of the cases discussed, the posterior on  $M_{\text{chirp}}$  is essentially unchanged, since this parameter is less strongly correlated with the others shown in the corner plot. Furthermore, similarly to the non-accreting case, the redshift of the source inferred from the luminosity distance does not change significantly with the choice of PBH-motivated priors.

Finally, the Bayes factors for GW190412 in the presence of accretion are  $\log \mathcal{B} = (143.4 \pm 0.2, 144.6 \pm 0.2, 145.5 \pm 0.2)$  for  $z_{\text{cut-off}} = (7, 10, 15)$ , respectively. These are to be compared with those obtained with standard (flat) priors ( $\log \mathcal{B} = 146.7 \pm 0.2$ ) and with PBH-motivated priors in the absence of accretion ( $\log \mathcal{B} = 144.8 \pm 0.2$ ), see Table 4. Overall, the Bayes factors do not disfavor the primordial origin of GW190412 significantly, especially in the moderately-weak accretion case. Nonetheless, it is important to stress that the Bayes factors for the case of accretion have been calculated using the approximate priors. We caution the reader that this could introduce a systematic error in the evidence calculation depending on how the approximation affects the whole prior volume (compared to the case of exact priors). However, quantifying this error would require a separate work and is beyond our scope here.

## 5 Conclusions

We have explored how assuming that (at least some of) the binary BH coalescences detected so far by the LVC have a primordial (rather than astrophysical) origin affects the binary parameters inferred through the GW data. PBHs are likely to be formed with a negligible spin and might possibly acquire some angular momentum only if an efficient phase of accretion at the (super)Eddington rate occurs during their cosmic history [37, 39]. These properties change the prior distributions of BH masses and spins relative to the agnostic (flat) distributions typically adopted. We performed a full Bayesian parameter estimation using PBH-motivated priors for some representative transient GW signals. In overall agreement with previous work [40–42], our results show that the choice of the priors can affect the measurements (and possibly the physical interpretation) of the binary BH parameters significantly for those events in which the standard LVC measurements are in tension with the new prior distribution, since the waveform parameters tend to ”readjust” in order to alleviate the tension with the new priors.

Our analysis allows to draw some general conclusions:

- The chirp mass of the binary and the source redshift are almost insensitive to the choice of a PBH-motivated priors, whereas the posterior distribution of the mass ratio and of the effective spin can be affected significantly for some binary BH systems.

- A prior with negligible-spin support (as suggested by the PBH scenario without accretion, or by a putative astrophysical scenario in which the supernova remnant is slowly spinning, or also if quantum effects at BH formation are relevant [43]) can strongly affect the overall parameter estimation of those binaries identified as spinning with a standard analysis that uses flat spin priors. In particular, at least for the cases we studied, the posterior distribution of the mass ratio gains more support close to unity relative to the standard case. Thus, binaries identified as (highly) spinning and (highly) asymmetrical by using standard agnostic priors might actually be non-spinning and symmetrical. Interestingly enough, for most of the events considered in this work the Bayes factor do not strongly favor one hypothesis against the other.
- A strong phase of accretion in the PBH history yields a bimodal prior distribution of the spin magnitudes, which is also mass- (and redshift-) dependent. Nonetheless, the distribution of  $\chi_{\text{eff}}$  is typically broad, owing to the broadness of the distribution of the individual masses (which propagates into  $\chi_{\text{eff}}$ , see Eq. (2.8)) and – most importantly – because the spin orientations are unknown. Even if both the masses and the spin magnitudes were known with infinite precision, the uncertainty on the spin orientations makes the prior distribution of  $\chi_{\text{eff}}$  broad, jeopardizing its constraining power in the case of strong accretion.
- Nonetheless, in the accreting case BH binaries tend to be symmetrical, so the prior on the mass ratio  $q$  is skewed towards unity. This might strongly affect the inference on  $q$  (and on  $\chi_{\text{eff}}$ , which is correlated to it) for those binaries identified as asymmetrical using agnostic priors, which is the case of GW190412.
- In particular, one of the main results of our analysis is that, if GW190412 is assumed to be of primordial origin, its mass ratio inferred from the data can be compatible with unity.

Many qualitative aspects of our analysis are valid beyond the PBH scenario. In particular, the above conclusions for the non-accreting PBH case (in which the priors implement the information that the PBH spins are essentially negligible) are also qualitatively valid for other scenarios in which the binary BHs are not necessarily of primordial origin but their spin is nonetheless small. In this case, we predict that the mass ratio of binaries identified as spinning using standard (flat) spin priors should be strongly affected and tend more towards unity to compensate for the absence of an effective spin term in the waveform model.

We also note that even if in the PBH scenario the physical parameters of some binaries are different from the standard ones, they do not affect a  $\chi^2$ -analysis of the PBH mass function significantly, so the analysis of Ref. [39] is not affected by our results.

Although we considered only a subset of the O1-O2-O3 LVC events, our analysis allows us to identify the key factors which are responsible for the impact of the priors also in other events. For example, the recent GW190814 [80] is a low-mass (with lighter companion in the low-mass gap and therefore prone to a PBH interpretation [19]), asymmetrical, non-spinning binary. Therefore, we expect that in this case the PBH-motivated priors should not affect the binary parameters significantly when accretion is negligible, whereas the inferred mass

ratio can be compatible with unity if accretion is strong. On the other hand, if the binary BH candidate GW190521g is confirmed as a high-mass binary [81] (with masses possibly in the high-mass gap), almost symmetrical binary with non-negligible spin [81], we predict that PBH-motivated priors in the absence of accretion would affect the inference on the system mass ratio. A detailed analysis of these events, as well as all others in the upcoming O3 catalogue, is left for future work.

Another interesting extension of our work is to compare the odds of the PBH hypothesis with those of different astrophysical scenarios, e.g. hierarchical mergers [82, 83], within the Bayesian framework used here.

## Acknowledgments

We thank the developers of BILBY code infrastructure, especially Greg Ashton, Colm Talbot, Moritz Hübner and Sylvia Biscoveanu for technical discussions on BILBY. Computations were performed at Sapienza University of Rome on the Vera cluster and at the University of Geneva on the Baobab cluster. V.DL., G.F. and A.R. are supported by the Swiss National Science Foundation (SNSF), project *The Non-Gaussian Universe and Cosmological Symmetries*, project number: 200020-178787. P.P. acknowledges financial support provided under the European Union’s H2020 ERC, Starting Grant agreement no. DarkGRA–757480, under the MIUR PRIN and FARE programmes (GW-NEXT, CUP: B84I20000100001), and support from the Amaldi Research Center funded by the MIUR program ‘Dipartimento di Eccellenza’ (CUP: B81I18001170001).

## A Parameter estimation for GW190412 in the accreting PBH scenario with $z_{\text{cut-off}} = 7$

For completeness in Fig. 11 we show the same corner plot for the posterior distributions of the parameters of GW190412 (see Fig. 10) but for the accreting PBH scenario with  $z_{\text{cut-off}} = 7$ . The results of this extreme scenario (in which accretion is efficient also at relatively small redshift) are qualitatively similar to the more likely case in which  $z_{\text{cut-off}} = 10$ , see Fig. 10 and discussion in the main text.

## References

- [1] LIGO SCIENTIFIC, VIRGO collaboration, B. P. Abbott et al., *GWTC-1: A Gravitational-Wave Transient Catalog of Compact Binary Mergers Observed by LIGO and Virgo* [\*Phys. Rev. X\* \*\*9\*\* \(2019\) 031040](#), [[1811.12907](#)].
- [2] LIGO SCIENTIFIC, VIRGO collaboration, R. Abbott et al., *GW190412: Observation of a Binary-Black-Hole Coalescence with Asymmetric Masses*, [\*Phys. Rev. D\* \*\*102\*\* \(2020\) 043015](#), [[2004.08342](#)].
- [3] M. Sasaki, T. Suyama, T. Tanaka and S. Yokoyama, *Primordial black holes—perspectives in gravitational wave astronomy*, [\*Class. Quant. Grav.\* \*\*35\*\* \(2018\) 063001](#), [[1801.05235](#)].

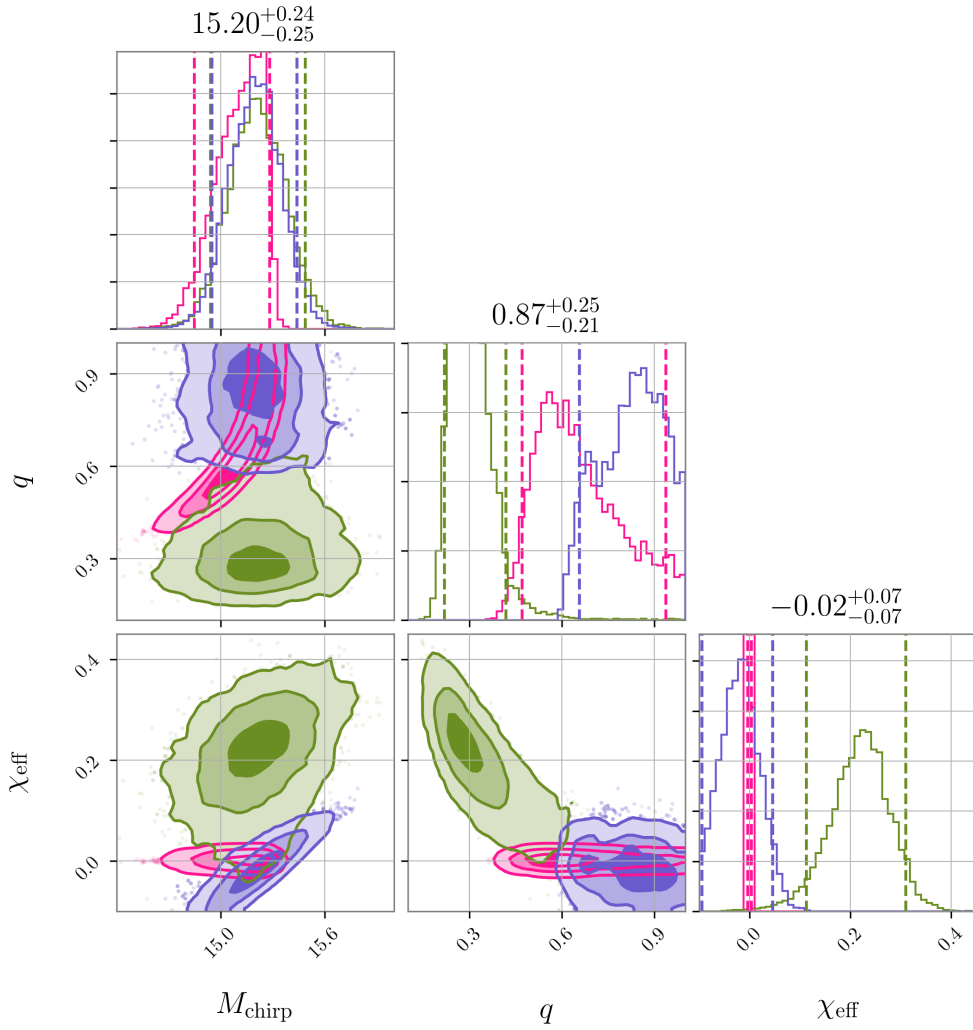


**Figure 11.** Same corner plot for GW190412 as in Fig. 10 but the accreting PBH scenario with  $z_{\text{cut-off}} = 7$ . The results are qualitatively similar to the other cases shown in Fig. 10.

- [4] A. M. Green and B. J. Kavanagh, Primordial Black Holes as a dark matter candidate, [2007.10722](#).
- [5] S. Bird, I. Cholis, J. B. Muñoz, Y. Ali-Haimoud, M. Kamionkowski, E. D. Kovetz et al., Did LIGO detect dark matter?, [Phys. Rev. Lett.](#) **116** (2016) 201301, [[1603.00464](#)].
- [6] M. Sasaki, T. Suyama, T. Tanaka and S. Yokoyama, Primordial Black Hole Scenario for the Gravitational-Wave Event GW150914, [Phys. Rev. Lett.](#) **117** (2016) 061101, [[1603.08338](#)].
- [7] B. Carr, K. Kohri, Y. Sendouda and J. Yokoyama, Constraints on Primordial Black Holes, [2002.12778](#).
- [8] S. Blinnikov, A. Dolgov, N. K. Porayko and K. Postnov, Solving puzzles of GW150914 by primordial black holes, [JCAP](#) **1611** (2016) 036, [[1611.00541](#)].
- [9] P. Ivanov, P. Naselsky and I. Novikov, Inflation and primordial black holes as dark matter,

- [Phys. Rev. D](#) **50** (1994) 7173–7178.
- [10] J. Garcia-Bellido, A. D. Linde and D. Wands, Density perturbations and black hole formation in hybrid inflation, [Phys. Rev. D](#) **54** (1996) 6040–6058, [[astro-ph/9605094](#)].
- [11] P. Ivanov, Nonlinear metric perturbations and production of primordial black holes, [Phys. Rev. D](#) **57** (1998) 7145–7154, [[astro-ph/9708224](#)].
- [12] Y. Ali-Haïmoud, E. D. Kovetz and M. Kamionkowski, Merger rate of primordial black-hole binaries, [Phys. Rev. D](#) **96** (2017) 123523, [[1709.06576](#)].
- [13] M. Raidal, C. Spethmann, V. Vaskonen and H. Veermäe, Formation and Evolution of Primordial Black Hole Binaries in the Early Universe, [JCAP](#) **02** (2019) 018, [[1812.01930](#)].
- [14] G. Hütsi, M. Raidal and H. Veermäe, Small-scale structure of primordial black hole dark matter and its implications for accretion, [Phys. Rev. D](#) **100** (2019) 083016, [[1907.06533](#)].
- [15] V. Vaskonen and H. Veermäe, Lower bound on the primordial black hole merger rate, [Phys. Rev. D](#) **101** (2020) 043015, [[1908.09752](#)].
- [16] K. Jedamzik, Primordial Black Hole Dark Matter and the LIGO/Virgo observations, [2006.11172](#).
- [17] K. Jedamzik, Evidence for primordial black hole dark matter from LIGO/Virgo merger rates, [2007.03565](#).
- [18] S. Young and A. S. Hamers, The impact on distant fly-bys on the rate of binary primordial black hole mergers, [2006.15023](#).
- [19] S. Clesse and J. Garcia-Bellido, GW190425 and GW190814: Two candidate mergers of primordial black holes from the QCD epoch, [2007.06481](#).
- [20] MACHO collaboration, R. A. Allsman et al., MACHO project limits on black hole dark matter in the 1-30 solar mass range, [Astrophys. J. Lett.](#) **550** (2001) L169, [[astro-ph/0011506](#)].
- [21] A. Kashlinsky, LIGO gravitational wave detection, primordial black holes and the near-IR cosmic infrared background anisotropy, [Astrophys. J. Lett.](#) **823** (2016) L25, [[1605.04023](#)].
- [22] Y. Ali-Haïmoud and M. Kamionkowski, Cosmic microwave background limits on accreting primordial black holes, [Phys. Rev. D](#) **95** (2017) 043534, [[1612.05644](#)].
- [23] M. Oguri, J. M. Diego, N. Kaiser, P. L. Kelly and T. Broadhurst, Understanding caustic crossings in giant arcs: characteristic scales, event rates, and constraints on compact dark matter, [Phys. Rev. D](#) **97** (2018) 023518, [[1710.00148](#)].
- [24] B. Carr, M. Raidal, T. Tenkanen, V. Vaskonen and H. Veermäe, Primordial black hole constraints for extended mass functions, [Phys. Rev. D](#) **96** (2017) 023514, [[1705.05567](#)].

- [25] N. Bellomo, J. L. Bernal, A. Raccanelli and L. Verde,  
Primordial Black Holes as Dark Matter: Converting Constraints from Monochromatic to Extended Mass Distributions, [JCAP](#) **01** (2018) 004, [[1709.07467](#)].
- [26] M. Zumalacarregui and U. Seljak,  
Limits on stellar-mass compact objects as dark matter from gravitational lensing of type Ia supernovae, [Phys. Rev. Lett.](#) **121** (2018) 141101, [[1712.02240](#)].
- [27] J. Manshanden, D. Gaggero, G. Bertone, R. M. Connors and M. Ricotti,  
Multi-wavelength astronomical searches for primordial black holes, [JCAP](#) **06** (2019) 026, [[1812.07967](#)].
- [28] H. Niikura, M. Takada, S. Yokoyama, T. Sumi and S. Masaki,  
Constraints on Earth-mass primordial black holes from OGLE 5-year microlensing events, [Phys. Rev.](#) **D99** (2019) 083503, [[1901.07120](#)].
- [29] R. Murgia, G. Scelfo, M. Viel and A. Raccanelli,  
Lyman- $\alpha$  Forest Constraints on Primordial Black Holes as Dark Matter, [Phys. Rev. Lett.](#) **123** (2019) 071102, [[1903.10509](#)].
- [30] Z.-C. Chen, C. Yuan and Q.-G. Huang,  
Pulsar Timing Array Constraints on Primordial Black Holes with NANOGrav 11-Year Data Set, [Phys. Rev. Lett.](#) **124** (2020) 251101, [[1910.12239](#)].
- [31] P. D. Serpico, V. Poulin, D. Inman and K. Kohri,  
Cosmic microwave background bounds on primordial black holes including dark matter halo accretion, [Phys. Rev. Res.](#) **2** (2020) 023204, [[2002.10771](#)].
- [32] V. De Luca, G. Franciolini, P. Pani and A. Riotto,  
Constraints on Primordial Black Holes: the Importance of Accretion, [2003.12589](#).
- [33] P. Lu, V. Takhistov, G. B. Gelmini, K. Hayashi, Y. Inoue and A. Kusenko,  
Constraining Primordial Black Holes with Dwarf Galaxy Heating, [2007.02213](#).
- [34] S. Clesse and J. García-Bellido,  
The clustering of massive Primordial Black Holes as Dark Matter: measuring their mass distribution with AdvLIGO, [Phys. Dark Univ.](#) **15** (2017) 142–147, [[1603.05234](#)].
- [35] Z.-C. Chen and Q.-G. Huang, Merger Rate Distribution of Primordial-Black-Hole Binaries, [Astrophys. J.](#) **864** (2018) 61, [[1801.10327](#)].
- [36] A. D. Gow, C. T. Byrnes, A. Hall and J. A. Peacock,  
Primordial black hole merger rates: distributions for multiple LIGO observables, [JCAP](#) **01** (2020) 031, [[1911.12685](#)].
- [37] V. De Luca, G. Franciolini, P. Pani and A. Riotto,  
The Evolution of Primordial Black Holes and their Final Observable Spins, [JCAP](#) **04** (2020) 052, [[2003.02778](#)].
- [38] A. Dolgov, A. Kuranov, N. Mitichkin, S. Porey, K. Postnov, O. Sazhina et al.,  
On mass distribution of coalescing black holes, [2005.00892](#).
- [39] V. De Luca, G. Franciolini, P. Pani and A. Riotto,  
Primordial Black Holes Confront LIGO/Virgo data: Current situation, [JCAP](#) **06** (2020) 044, [[2005.05641](#)].
- [40] S. Vitale, D. Gerosa, C.-J. Haster, K. Chatziioannou and A. Zimmerman,

- Impact of Bayesian Priors on the Characterization of Binary Black Hole Coalescences, [Phys. Rev. Lett.](#) **119** (2017) 251103, [[1707.04637](#)].
- [41] I. Mandel and T. Fragos, [An alternative interpretation of GW190412 as a binary black hole merger with a rapidly spinning secondary](#), [Astrophys. J.](#) **895** (2020) L28, [[2004.09288](#)].
- [42] M. Zevin, C. P. Berry, S. Coughlin, K. Chatziioannou and S. Vitale, [You Can Always Get What You Want: The Impact of Prior Assumptions on Interpreting GW190412](#), [2006.11293](#).
- [43] E. Bianchi, A. Gupta, H. M. Haggard and B. Sathyaprakash, [Quantum gravity and black hole spin in gravitational wave observations: a test of the Bekenstein-Hawking entropy bound](#), [1812.05127](#).
- [44] A. Dolgov and J. Silk, [Baryon isocurvature fluctuations at small scales and baryonic dark matter](#), [Phys. Rev. D](#) **47** (1993) 4244–4255.
- [45] J. M. Bardeen, J. Bond, N. Kaiser and A. Szalay, [The Statistics of Peaks of Gaussian Random Fields](#), [Astrophys. J.](#) **304** (1986) 15–61.
- [46] V. De Luca, V. Desjacques, G. Franciolini, A. Malhotra and A. Riotto, [The initial spin probability distribution of primordial black holes](#), [JCAP](#) **1905** (2019) 018, [[1903.01179](#)].
- [47] M. Mirbabayi, A. Gruzinov and J. Noreña, [Spin of Primordial Black Holes](#), [JCAP](#) **2003** (2020) 017, [[1901.05963](#)].
- [48] M. Ricotti, [Bondi accretion in the early universe](#), [Astrophys. J.](#) **662** (2007) 53–61, [[0706.0864](#)].
- [49] M. Ricotti, J. P. Ostriker and K. J. Mack, [Effect of Primordial Black Holes on the Cosmic Microwave Background and Cosmological Parameter Estimates](#), [Astrophys. J.](#) **680** (2008) 829, [[0709.0524](#)].
- [50] J. R. Rice and B. Zhang, [Cosmological evolution of primordial black holes](#), [JHEAp](#) **13-14** (2017) 22–31, [[1702.08069](#)].
- [51] E. Berti and M. Volonteri, [Cosmological black hole spin evolution by mergers and accretion](#), [Astrophys. J.](#) **684** (2008) 822–828, [[0802.0025](#)].
- [52] J. Adamek, C. T. Byrnes, M. Gosenca and S. Hotchkiss, [WIMPs and stellar-mass primordial black holes are incompatible](#), [Phys. Rev. D](#) **100** (2019) 023506, [[1901.08528](#)].
- [53] K. J. Mack, J. P. Ostriker and M. Ricotti, [Growth of structure seeded by primordial black holes](#), [Astrophys. J.](#) **665** (2007) 1277–1287, [[astro-ph/0608642](#)].
- [54] V. Bosch-Ramon and N. Bellomo, [Mechanical feedback effects on primordial black hole accretion](#), [Astron. Astrophys.](#) **638** (2020) A132, [[2004.11224](#)].
- [55] S. P. Oh and Z. Haiman, [Fossil HII regions: Self-limiting star formation at high redshift](#), [Mon. Not. Roy. Astron. Soc.](#) **346** (2003) 456, [[astro-ph/0307135](#)].
- [56] G. Hasinger, [Illuminating the dark ages: Cosmic backgrounds from accretion onto primordial black hole dark matter](#), [2003.05150](#).

- [57] G. Hütsi, M. Raidal and H. Veermäe, Small-scale structure of primordial black hole dark matter and its implications for accretion, [\*Phys. Rev. D\* \*\*100\*\* \(2019\) 083016](#), [[1907.06533](#)].
- [58] N. I. Shakura and R. A. Sunyaev, Black holes in binary systems. Observational appearance, *Astron. Astrophys.* **24** (1973) 337–355.
- [59] I. D. Novikov and K. S. Thorne, Astrophysics of black holes., in Black Holes (Les Astres Occlus), pp. 343–450, Jan., 1973.
- [60] J. M. Bardeen, W. H. Press and S. A. Teukolsky, Rotating black holes: Locally nonrotating frames, energy extraction, and scalar synchrotron radiation, [\*Astrophys. J.\* \*\*178\*\* \(1972\) 347](#).
- [61] R. Brito, V. Cardoso and P. Pani, Black holes as particle detectors: evolution of superradiant instabilities, [\*Class. Quant. Grav.\* \*\*32\*\* \(2015\) 134001](#), [[1411.0686](#)].
- [62] M. Volonteri, P. Madau, E. Quataert and M. J. Rees, The Distribution and cosmic evolution of massive black hole spins, [\*Astrophys. J.\*](#) , [[astro-ph/0410342](#)].
- [63] K. S. Thorne, Disk accretion onto a black hole. 2. Evolution of the hole., [\*Astrophys. J.\* \*\*191\*\* \(1974\) 507–520](#).
- [64] C. F. Gammie, S. L. Shapiro and J. C. McKinney, Black hole spin evolution, [\*Astrophys. J.\* \*\*602\*\* \(2004\) 312–319](#), [[astro-ph/0310886](#)].
- [65] V. Vaskonen and H. Veermäe, Lower bound on the primordial black hole merger rate, [\*Phys. Rev. D\* \*\*101\*\* \(2020\) 043015](#), [[1908.09752](#)].
- [66] L. Blanchet, Gravitational Radiation from Post-Newtonian Sources and Inspiralling Compact Binaries, [\*Living Rev. Rel.\* \*\*17\*\* \(2014\) 2](#), [[1310.1528](#)].
- [67] L. Xiang, A review of: “introduction to bayesian statistics”, [\*IIE Transactions\* \*\*39\*\* \(2007\) 829–829](#), [<https://doi.org/10.1080/07408170600941656>].
- [68] I. Romero-Shaw et al., Bayesian inference for compact binary coalescences with BILBY: Validation and application to the first LIGO–V, [2006.00714](#).
- [69] G. Ashton et al., BILBY: A user-friendly Bayesian inference library for gravitational-wave astronomy, [\*Astrophys. J. Suppl.\* \*\*241\*\* \(2019\) 27](#), [[1811.02042](#)].
- [70] J. S. Speagle, DYNESTY: a dynamic nested sampling package for estimating Bayesian posteriors and evidences, [\*Mon. Not. R. Astron. Soc\* \*\*493\*\* \(Apr., 2020\) 3132–3158](#), [[1904.02180](#)].
- [71] J. Skilling, Nested sampling for general bayesian computation, [\*Bayesian Anal.\* \*\*1\*\* \(12, 2006\) 833–859](#).
- [72] J. Skilling, Nested Sampling, in American Institute of Physics Conference Series (R. Fischer, R. Preuss and U. V. Toussaint, eds.), vol. 735 of American Institute of Physics Conference Series, pp. 395–405, Nov., 2004. DOI.
- [73] T. L. S. Collaboration and the Virgo Collaboration, Gw190412: Observation of a binary-black-hole coalescence with asymmetric masses, 2020.

- [74] LIGO Scientific Collaboration, “LIGO Algorithm Library - LALSuite.” free software (GPL), 2018. 10.7935/GT1W-FZ16.
- [75] M. Walker, A. F. Agnew, J. Bidler, A. Lundgren, A. Macedo, D. Macleod et al., Identifying correlations between ligo’s astronomical range and auxiliary sensors using lasso regression, [\*Classical and Quantum Gravity\* \*\*35\*\* \(Oct, 2018\) 225002](#).
- [76] S. Coughlin, S. Bahaadini, N. Rohani, M. Zevin, O. Patane, M. Harandi et al., Classifying the unknown: Discovering novel gravitational-wave detector glitches using similarity learning, [\*Phys. Rev. D\* \*\*99\*\* \(Apr, 2019\) 082002](#).
- [77] LIGO SCIENTIFIC, VIRGO collaboration, B. Abbott et al., Observation of Gravitational Waves from a Binary Black Hole Merger, [\*Phys. Rev. Lett.\* \*\*116\*\* \(2016\) 061102](#), [[1602.03837](#)].
- [78] LIGO SCIENTIFIC, VIRGO collaboration, B. P. Abbott et al., GW170608: Observation of a 19-solar-mass Binary Black Hole Coalescence, [\*Astrophys. J.\* \*\*851\*\* \(2017\) L35](#), [[1711.05578](#)].
- [79] K. Chatzioannou et al., On the properties of the massive binary black hole merger GW170729, [\*Phys. Rev. D\* \*\*100\*\* \(2019\) 104015](#), [[1903.06742](#)].
- [80] LIGO SCIENTIFIC, VIRGO collaboration, R. Abbott et al., GW190814: Gravitational Waves from the Coalescence of a 23 Solar Mass Black Hole with a 2.6 Solar Mass Companion, [\*Astrophys. J.\* \*\*896\*\* \(2020\) L44](#), [[2006.12611](#)].
- [81] M. Graham et al., Candidate Electromagnetic Counterpart to the Binary Black Hole Merger Gravitational Wave Event S190521g, [\*Phys. Rev. Lett.\* \*\*124\*\* \(2020\) 251102](#), [[2006.14122](#)].
- [82] D. Gerosa and E. Berti, Are merging black holes born from stellar collapse or previous mergers?, [\*Phys. Rev. D\* \*\*95\*\* \(2017\) 124046](#), [[1703.06223](#)].
- [83] D. Gerosa, S. Vitale and E. Berti, Astrophysical implications of GW190412 as a remnant of a previous black-hole merger, [2005.04243](#).